

# M agnitude-D ependent O m ori L aw : E m p i r i c a l S t u d y a n d T h e o r y

G . O u i l l o n a n d D . S o m e t t e

D e p a r t m e n t o f E a r t h a n d S p a c e S c i e n c e s a n d I n s t i t u t e o f G e o p h y s i c s a n d P l a n e t a r y P h y s i c s ,

U n i v e r s i t y o f C a l i f o r n i a , L o s A n g e l e s , C a l i f o r n i a 90095-1567 a n d L a b o r a t o i r e d e P h y s i q u e d e l a M a t i e r e

C o n d e n s e e , C N R S U M R 6622 U n i v e r s i t e d e N i c e - S o p h i a A n t i p o l i s , P a r c V a l r o s e , 06108 N i c e , F r a n c e

Short title: M A G N I T U D E - D E P E N D E N T O M O R I L A W

Abstract.

We propose a new physically-based "multifractal stress activation" model of earthquake interaction and triggering based on two simple ingredients: (i) a seismic rupture results from activated processes giving an exponential dependence on the local stress; (ii) the stress relaxation has a long memory. The combination of these two effects predicts in a rather general way that seismic decay rates after mainshocks follow the Omori law  $\dot{\lambda} = p$  with exponents  $p$  linearly increasing with the magnitude  $M_L$  of the mainshock and the inverse temperature. We carefully test the prediction on the magnitude dependence of  $p$  by a detailed analysis of earthquake sequences in the Southern California Earthquake catalog. We find power law relaxations of seismic sequences triggered by mainshocks with exponents  $p$  increasing with the mainshock magnitude by approximately  $0.1 \pm 0.15$  for each magnitude unit increase, from  $p(M_L = 3) = 0.6$  to  $p(M_L = 7) = 1.1$ , in good agreement with the prediction of the multifractal model. The results are robust with respect to different time intervals, magnitude ranges and declustering methods. When applied to synthetic catalogs generated by the ETAS (Epidemic-Type Aftershock Sequence) model constituting a strong null hypothesis with built-in magnitude-independent  $p$ -values, our procedure recovers the correct magnitude-independent  $p$ -values. Our analysis thus suggests that a new important fact of seismicity has been unearthed. We discuss alternative interpretations of the data and describe other predictions of the model.

## 1. Introduction

There are now many evidences that the space-time organization of earthquakes is consistent with the idea that a single physical triggering mechanism is responsible for the occurrence of aftershocks, mainshocks, foreshocks, and multiplets, leading to the more encompassing concept of earthquake triggering (see for instance [Lin and Stein, 2004; Feltzer et al., 2004; Murru et al., 2004; Huc and Main, 2003; Marsan, 2003; Helmstetter and Somette, 2003; Papazachos et al., 2000]).

Earthquake triggering has been modeled using a variety of approaches including, static stress transfer calculations [King et al., 1994; Stein, 2003], dynamic triggering processes [Voisin, 2002; Perfettini et al., 2003], as well as more phenomenological epidemic-type aftershock sequence (ETAS) models [Kagan and Knopov, 1981; 1987; Ogata, 1988] which are based on "mutually self-excited point processes" introduced by Hawkes [1971] (see [Helmstetter and Somette, 2002a] for properties of the ETAS model and a review of the literature). The later modeling approach in particular has been able to rationalize most of the phenomenological statistical properties of earthquake catalogs, such as the larger proportion than normal of large versus small foreshocks, the power law acceleration of stacked seismicity rate as a function of time to the mainshock, the spatial migration of foreshocks toward the mainshock when averaging over many sequences, the independence of foreshocks precursory properties as a function of the mainshock size, the existence of correlations in seismicity over surprisingly large length scales [Helmstetter and Somette, 2003a], Bath's law [Helmstetter and Somette, 2003b] and so on.

Its appeal due to the simplicity of its premise, its power of explanation of a large set of empirical observations and the relative ease with which it can be implemented for rigorous statistical tests has made the class of ETAS models the natural null hypothesis against which to test any other model of seismicity. The class of ETAS models suffers however from a major drawback, that is, the lack of a clear physical basis. The ETAS model is a statistical phenomenological construction which postulates a dependence of the present seismic rate on past seismic rates propagated forward in time via a bare Omori propagator.

One would thus like models in which seismic rates derive from the interaction between and transfer

of physical fields, such as stress, strain rates and fluid flows. For this purpose, we present here a generalization which has a sound physical basis, as it relies on two fundamental physical ingredients: rupture activation and stress transfer. Rupture activation is described by the generic thermal activation processes at the origin of the state- and velocity-dependent friction laws, stress corrosion effects, and so on. In the description of stress transfer, we take into account the long-time memory effects in the relaxation of stress fields due to the visco-elasto-plastic rheology of the crust and upper mantle. Using this model, we predict a new phenomenon, the dependence of the exponent  $p$  of the Omori law on the mainshock magnitude. This prediction is tested successfully by a careful analysis of the Southern California earthquake catalog. For this and for other reasons that will become clear below, we coin our model the "multifractal stress activation" model.

The organization of this paper is the following. In section 2, we first discuss the fundamental physical ingredients of the "multifractal stress activation" model. Section 3 gives its detailed definition. Section 4 shows by analytical calculations that the Omori law  $\dot{\epsilon} \propto t^{-1}$  derives naturally from the model, but with an exponent  $p$  which is an increasing linear function of the mainshock magnitude. This surprising prediction results from the interplay between the exponential activation process and the long-time memory of stress relaxation processes. Section 5 tests this prediction using different declustering techniques to identify mainshocks at magnitudes ranging from 1.5 to 7.5 in the Southern California catalog and to stack their corresponding aftershock sequences. We find a remarkable agreement with  $p(M)$  increasing from approximately  $p = 0.6$  for  $M = 3$  to  $p = 1.1$  for  $M = 7$ . We also present tests on synthetic catalogs generated with the ETAS model. Section 6 presents other observations that can be reinterpreted within the framework of our model and discuss other predictions.

## 2. Fundamentals of the "multifractal stress activation" model

### 2.1. Earthquakes as thermally activated processes

We model seismic activity as the occurrence of frictional sliding events and/or fault ruptures that are thermally activated processes facilitated by the applied stress field. The relevance of thermal activation is made clear when examining the underlying physical processes of the various proposed models of earthquakes, which we now briefly review.

Thermal activation is known to control creep rupture (also called static fatigue) (see for instance the review in [Scholz, 2002] for the application to rock mechanics and to earthquakes and [Ciliberto et al., 2001; Politi et al., 2002; Saichev and Sornette, 2003] for recent experimental and theoretical developments).

The use of the Eyring rheology and other thermally-dependent friction laws are of standard use for describing creep failure in a variety of compounds [Liu and Ross, 1996] as well as material interfaces [Mulliet, 2000]. These laws consist in adapting, at the microscopic level, the theory of reaction rates describing processes activated by crossing potential barriers.

Stress corrosion occurs in the presence of pre-existing cracks in quartz, quartz rocks, calcite rocks, basaltic rocks, granitic rocks and many other geological materials [Atkinson et al., 1981; Atkinson, 1984] by the mechanism of hydrolytic weakening [Griggs et al., 1957; Griggs and Handin, 1960] which is also thermally activated (see [Sornette, 1999] for a review and references therein).

The Ruina-Dieterich state-and-velocity dependent friction law [Dieterich, 1979; Ruina, 1983; Scholz, 1998] results physically from creep of the surface contact and a consequent increase in real contact area with time of contact [Scholz and Engelder, 1976; Wang and Scholz, 1994]. The logarithmic form  $\ln V$  of the velocity dependence of the friction coefficient in the Ruina-Dieterich law is usually assumed to derive from an Arrhenius activated rate process describing creep at asperity contacts [Stesky, 1977; Chester and Higgs, 1992; Chester, 1994; Heslot et al., 1994;

Brechet and Estrin, 1994; Baumberger, 1997; Sleep, 1997; Persson, 1998; Baumberger et al., 1999; Lapusta et al., 2000; Nakatani, 2001].

## 2.2. Long-time memory effects in the relaxation of stress fields

A recent re-construction of the regional strain rate map in California from GPS recordings over a dense network shows that the largest strain rates are controlled by past large earthquakes and are found in the regions where aftershock activity is still noticeable [Jackson et al., 1997]. This suggests the relevance of a stress-controlled earthquake activation. Post-seismic slip and strain rate relaxation following large earthquakes have been modeled by visco-elastic flows, which govern the evolution of the stress field and thus the loading and unloading processes of major earthquake generating faults [Deng et al., 1998]. The simplest models assume linear visco-elastic rheologies, which lead to exponential strain relaxation. These models in general account for the short-term relaxation processes over a time scale ranging from a few months to one year [Pollitz et al., 2000]. Over long time scales, it is necessary to take into account the presence and geometry of lower crustal and mantle shear zones, which lead to more complex and slower decaying relaxation rates [Kenner and Segall, 1999]. To adequately model long-term postseismic relaxation (i.e. that occurring years to decades after an earthquake) for instance after the Landers and Hector Mine earthquakes, it was found necessary to add other slower deformation processes [Freed and Lin, 2000; 2001]. Evidence of large post-seismic relaxation times have been found within the crust in the case of slow-rate intracontinental events [Calais et al., 2002]. Long-term stress relaxation processes are also found in empirical laws of creep experiments applied to model the brittle creeping fault zone, which can account for both the time evolution of afterslip, as measured from geodesy, and of aftershocks decay. In this framework, aftershock sequences and deep afterslip, as constrained from geodetic measurements, follow the same temporal evolution [Perfettini and Avouac, 2004]. Generally, slower-than-exponential relaxation is found in disordered materials which can be characterized by nonlinear rheologies [Klinger, 1988; Chung and Stevens, 1991; Phillips, 1996].

### 3. Formulation of the "multifractal stress activation" model

#### 3.1. General case

Let us denote by  $\lambda(\mathbf{x};t)$  the intensity (or average conditional seismicity rate) at position  $\mathbf{x}$  and time  $t$ . Putting together the two physical ingredients of rupture activation and stress transfer discussed above, we formulate the following model. The thermal rupture activation process is expressed as

$$\lambda(\mathbf{x};t) = \exp[-E(\mathbf{x};t)] ; \quad (1)$$

where  $\beta$  is the inverse temperature (speci cally  $\beta = 1/kT$  where  $k$  is the Boltzmann constant) and the energy barrier  $E(\mathbf{x};t)$  for rupture can be written as the sum of a contribution  $E_0(\mathbf{x})$  characterizing the material and of a term linearly decreasing with the locally applied stress  $\sigma(\mathbf{x};t)$  [Zhurkov, 1965]:

$$E(\mathbf{x};t) = E_0(\mathbf{x}) - V \sigma(\mathbf{x};t) ; \quad (2)$$

$V$  is a constant which has the dimension of a volume and  $\sigma(\mathbf{x};t)$  is the total stress at position  $\mathbf{x}$  and time  $t$ . The decrease of the energy barrier  $E(\mathbf{x};t)$  as a function of the applied stress  $\sigma(\mathbf{x};t)$  in (2) embodies the various physical processes of stress corrosion, state-and-velocity dependent friction and mechano-chemical effects, aiding rupture activation under stress. The stress  $\sigma(\mathbf{x};t)$  results itself from all past events according to

$$\sigma(\mathbf{x};t) = \sigma_{\text{far field}}(\mathbf{x};t) + \int_0^t \int_{\mathcal{V}} dN[\mathbf{x}^0, d] (\mathbf{x}^0) g(\mathbf{x} - \mathbf{x}^0; t - t^0) ; \quad (3)$$

Putting all this together yields

$$\lambda(\mathbf{x};t) = \lambda_{\text{tec}}(\mathbf{x};t) \exp \left[ \beta \int_0^t \int_{\mathcal{V}} dN[\mathbf{x}^0, d] (\mathbf{x}^0) g(\mathbf{x} - \mathbf{x}^0; t - t^0) \right] ; \quad (4)$$

In this expression, the term  $\lambda_{\text{tec}}$  now incorporates the volume term  $V$  and the inverse temperature ( $\beta = V/kT$ ), so that  $\beta$  has now the dimension of the inverse of a stress. The double integral gives the stress at position  $\mathbf{x}$  and time  $t$  as the sum of the stress load contributions over all past earthquakes at earlier times  $t^0 < t$  and positions  $\mathbf{x}^0$ . A given past event at  $\mathbf{x}^0$  and time  $t^0$  contributes to the stress at  $\mathbf{x}$  and time  $t$  by its stress drop amplitude  $\Delta\sigma(\mathbf{x}^0)$  which is transferred in space and time via the

stress kernel (or Green function)  $g(\mathbf{r} - \mathbf{r}^0; t - t^0)$ , taking into account both time relaxation and spatial geometrical decay. The kernel  $g(\mathbf{r} - \mathbf{r}^0; t - t^0)$  describes the combined effects of all stress relaxation processes in space and time, that determine the stress field in the seismogenic layer, as discussed in section 2.2. The term  $dN[\mathbf{r}^0 \in d\mathbf{r}^0]$  is the number of events in the volume  $d\mathbf{r}^0$  that occurred between  $t^0$  and  $t^0 + dt^0$ . Finally,  $\lambda_{\text{tec}}(\mathbf{r}; t)$  is the spontaneous seismicity rate in absence of stress triggering by other earthquakes and accounts for the tectonic loading (far field stress), which may in general be non-homogeneous and space and perhaps depends on time.

It is convenient to discretize space in cells and rewrite (4) as

$$\lambda_i(t) = \lambda_{\text{tec}}(t) \exp \left[ \sum_j \Delta \sigma_j(t) g_{ij}(t) \right]; \quad (5)$$

where  $\lambda_i(t)$  is the average conditional seismic rate in cell  $i$  at time  $t$ ,  $\Delta \sigma_j(t)$  is the stress drop in cell  $j$  that occurred at time  $t$  due to an earthquake and  $g_{ij}(t)$  measures the fraction of the stress drop that occurred at time  $t$  in cell  $j$  which is transferred to cell  $i$  at time  $t$ .

Our model (4,5) is reminiscent of the stress release model, but there are several important differences that are worth noting. The single cell stress release model was introduced by Vere-Jones [1978] as a stochastic implementation of Reid's theory of elastic rebound theory [Reid, 1910]. The generalization to account for long-range elastic stress transfer was done in [Zheng and Vere-Jones, 1991] and in [Liu et al., 1998; Shi et al., 1998] (see [Bebbington and Harte, 2003] for a review and references therein). The most general form of the stress release model (SRM) reads

$$\lambda_i(t) = \lambda_0 \exp \left[ b_1 t - b_2 \sum_j g_{ij} S_j(t) \right]; \quad (6)$$

In the SRM, the tectonic loading increases the stress at cell  $i$  linearly in time according to  $b_1 t$  and earthquakes on this cell and elsewhere relax (or load) the stress at cell  $i$ .  $S_j(t) = \sum_{t^0 \leq t} \Delta \sigma_j(t^0)$  is the cumulative stress release over all past earthquakes that occurred in that cell  $j$ .  $S_j(t)$  impacts region  $i$  through the time-independent coupling (or stress transfer) coefficient  $g_{ij}$ . In our model, the tectonic loading appears in contrast through the rate  $\lambda_{\text{tec}}(\mathbf{r}; t)$ . The SRM views the earthquakes as mostly unloading this tectonic stress (of course stress load is possible) while we view the earthquakes more



symmetrically as both promoting or shadowing the seismic activity elsewhere around an average rate controlled by  $\dot{\epsilon}_{\text{tec}}(\mathbf{x};t)$ . Finally, the most important difference lies in the fact that the SRM assumes an infinite time memory of past stress releases in the cumulative stress release function  $S_j(t)$ , while we view the stress transfer by each past earthquake as transient due to visco-elastic processes in the crust and mantle. This infinite time memory of the SRM is made necessary to compensate for the tectonic loading but in order to obtain a statistically stationary process. In contrast, our model is better devised to deal with transient stress perturbations induced by past earthquakes. As a consequence, the SRM is not built to produce aftershocks (see however the two-cells version of [Borokov and Bebbington, 2003], which does produce first generation aftershocks obeying the Omori law). The fits of seismic catalogs to the SRM indeed use declustered data. Thus, the fundamental difference between our model (4,5) and the linked SRM (6) is that the latter does not describe either aftershocks or delayed triggered seismicity (Imoto et al. [1999] introduced a fixed one-time delay in order to produce periodic-type behavior). Our model (4,5) is an important generalization to account for the delayed triggering processes, which have been found to explain many phenomenological observations of seismicity [Helmstetter and Somette, 2003a]. Actually, all the results that we derive below derive from the time-dependent memory kernel of our model, which are thus absent in the SRM.

### 3.2. Reduction to time-only dynamics

Starting from (4), we write the space-time kernel  $g(\mathbf{x};t)$  in a separable form

$$g(\mathbf{x};t) = f(\mathbf{x}) \cdot h(t) : \quad (7)$$

This choice is made for the sake of simplicity and is in the spirit of the specification of the ETAS which also assumes separability of the bare kernel in space and time. Helmstetter and Somette [2002b] have shown that the cascade of triggering of events which are decoupled in time and space in their first generation eventually leads to a coupling in space and time corresponding to a sub-division process. Here, we expect a similar mechanism to operate when taking into account all generations of earthquake triggering (a mainshock generates aftershocks of first-generation, which themselves trigger aftershocks

of second-generation and so on).

With the separable form (7), expression (4) can be transformed into

$$g(\mathbf{x};t) = g_{\text{tec}}(\mathbf{x};t) \exp \int_0^t \int_{\mathcal{D}} s(\mathbf{x};\mathbf{x}') h(t-t') d\mathbf{x}' dt' ; \quad (8)$$

where

$$s(\mathbf{x};\mathbf{x}') = \int_{\mathcal{D}} d\mathbf{x}'' g(\mathbf{x}' - \mathbf{x}'') f(\mathbf{x} - \mathbf{x}'') \quad (9)$$

is the effective source at time  $t$  at point  $\mathbf{x}$  resulting from all events occurring in the spatial domain at the same time  $t$ . The separable form of the kernel  $g(\mathbf{x};t)$  in (7) allows us to study the time-dependent properties of the model, independently of its space properties. Since expression (8) is defined for any  $\mathbf{x}$ , if we assume space homogeneity, or if we restrict to a specific domain, we can drop the reference to  $\mathbf{x}$  without loss of generality and get

$$g(t) = g_{\text{tec}}(t) \exp \int_0^t \int_{\mathcal{D}} s(\mathbf{x}) h(t-t') d\mathbf{x} dt' : \quad (10)$$

In contrast with the ETAS model in which the time-only equation of the conditional Poisson rate describes the seismicity integrated over all space, here the time-only equation (10) refers to a specific location. If space is homogeneous ( $g_{\text{tec}}(\mathbf{x};t)$  and  $s(\mathbf{x};\mathbf{x}')$  are independent of  $\mathbf{x}$ ), then equation (10) gives the conditional seismic Poisson intensity at any point.

### 3.3. The distribution of stress source strengths

The fact that the source is given by (9) should allow us to constrain its statistics. Indeed, Kagan [1994] has suggested using theoretical calculations, simulations and measurements of rotation of earthquake focal mechanisms that the stress change in earthquake focal zones due to past earthquakes should follow the symmetric Cauchy distribution

$$L_1(x) = \frac{1}{\pi} \frac{1}{1+x^2} ; \quad (11)$$

or perhaps even distributions decaying as power laws with even smaller exponents. The Cauchy distribution is a stable Levy law with power law tail exponent  $\alpha = 1$  and can be shown to be the

distribution for the stress at any point due to a random uniform distribution of sources mediated to that point via the elastic Green function [Zobtarev and Strunin, 1971; Zobtarev, 1986] (see also [Somette, 2004], chap. 17, for a general presentation). The physical mechanism for the Cauchy distribution is thus precisely the summation (9) over earthquake sources  $(\mathbf{x}^0)$  with stress transfer given by the elastic Green function  $f(\mathbf{x} - \mathbf{x}^0)$  in the crust. The Cauchy exponent  $\alpha = 1$  is obtained for a uniform spatial distribution of sources in 3D with the elastic Green function  $1=r^3$  in 3D, or for a uniform spatial distribution of sources in 2D with the elastic Green function  $1=r^2$  in 2D. For sources on a fractal with dimension  $D_f = 3$ ,  $\alpha = D_f = 3$  in 3D [Kagan, 1994].

However, it must be kept in mind that the large values of the stress sources  $s$  that contribute to the slow power law decay of the Cauchy distribution result from the assumption that earthquakes are point-wise such that a probe put at random in the medium can come arbitrarily close to these sources: it is the divergence  $1=r^3$  (in 3D) of the stress field close to such a singular source which is at the origin of the Cauchy distribution (see Chap. 17 of [Somette, 2004]). In reality, such singular power law behavior transforms into a much weaker  $1=r^p$  singularity close to crack tips and then crosses over to a smooth behavior due to plasticity and damage that smooth out the singularity sufficiently close to the fault edges.

To capture in a phenomenological way these features, we will use a power law distribution of the source strengths

$$P(s) = \frac{C}{(s^2 + s_0^2)^{\frac{1+\alpha}{2}}} = \frac{C}{s^{1+\alpha}} \quad (12)$$

where the scale factor  $C$  is given by  $C / s_0$  and  $s_0$  is a characteristic scale proportional to the average stress drop. The value  $\alpha = 1$  recovers the special case of the Cauchy distribution advocated by Kagan [1994]. Notice that the distribution of the source strengths is symmetric, implying that the effect of an earthquake in the past can either enhance or shadow the present seismicity. This generalizes the ETAS model as both stress triggering and stress shadowing are taken into account symmetrically while the ETAS model describes only stress triggering.

### 3.4. Time-dependent stress relaxation kernel

The last ingredient we need to specify is the time dependence of the memory kernel  $h(t)$ . We postulate a stress relaxation function

$$h(t) = \frac{h_0}{(t+c)^{1+}} ; \quad \text{for } 0 < t \leq T ; \quad (13)$$

which is of the Omori form with the usual small time-scale cut-off  $c$ . To ensure convergence of the correlation function of deterministic processes with memory governed by  $h(t)$  for any possible values of  $\alpha$ , we truncate the power law in (13) at some large time  $T$ , which we call the "integral time scale": it is the largest time scale up to which the memory of a past event survives.  $T$  can thus be interpreted as the effective Maxwell time of the relaxation process. The sharp cut-off implied by  $T$  is invoked for convenience and can be replaced by a smooth cross-over using for instance an exponential rolloff of the form

$$h(t) = \frac{h_0}{(t+c)^{1+}} e^{-t/T} ; \quad (14)$$

without changing our main conclusions below.

Just after an event over a time scale slightly larger than the time for the propagation and attenuation of dynamical stress waves, that we note  $t = 0^+$  for short, the stress equilibrates to its static value and we should have

$$h(0^+) = \frac{h_0}{c^{1+}} = 1 ; \quad (15)$$

to express that the static stress has not had time to relax yet.

Expressions (13) or (14) can be rationalized from the time dependence of the visco-elastic Green function in 1D which gives  $\alpha = 1/2$ , in 2D which gives  $\alpha = 0$  or in 3D which gives  $\alpha = 1/2$ . In fact, a better formulation will require a space-time dependence of the evolution of the stress field. Another argument is to view local stress as proportional to the local strain rate, which is itself proportional to the local microscopic seismic rate which obeys the Omori law. From a micro-mechanical point of view, such slow relaxation process (13) are associated with dislocation motion, stress corrosion and hydrolytic weakening processes [Somette, 1999]. We also would like to underline that expression (13) implies

the absence of a well-defined characteristic time scale for  $c < t < T$  where  $c \ll T$ , and embodies the complex non-Maxwell relaxation processes in the crust, its coupling with the lower visco-elasto-plastic crust and more ductile upper mantle. The coexistence of many different time scales can be captured by such power law decay.

Actually, there is a more profound origin of the dependence (13) of the stress relaxation. Assume that an earthquake loads a given region according to the elastic stress redistribution that can be estimated using standard methods of elasticity [King et al., 1994; Stein, 2003]. Then, by the activation processes discussed in section 2.1, this stress redistribution induced by the "mainshock" will give rise to an increase of seismicity at that region. The triggered earthquakes will lead to new sources of stress redistribution, which themselves modify the stress field, tending to decrease it. This process gives rise to a slow power law relaxation of the stress field [Lee and Somette, 2000]. The power law decay embodied in (13) can thus be viewed as resulting from the microscopic process of stress redistribution and relaxation which occur below the scale of observation. There is no reason for the physics to change and this law (13) is an effective renormalization of many microscopic relaxation processes.

### 3.5. Summary of the model definition

Summarizing, in a discrete form, our model reads

$$\sigma(t) = \sigma_{tec} \exp \left[ - \sum_{i: t_i \leq t} s(t_i) h(t - t_i)^5 \right]; \quad (16)$$

where the stress at time  $t$  is the sum of the contributions over all previous earthquakes that occurred at times  $t_i \leq t$ , with stress sources given by the power law distribution (12) and with a power law time-dependent stress relaxation kernel (13). In the sequel, we take a constant seismic rate  $\sigma_{tec}$  in the absence of stress perturbation  $s(t_i) = 0$ .

It is convenient to rewrite (16) as

$$\sigma(t) = \sigma_{tec} e^{-\phi(t)}; \quad (17)$$

where

$$\lambda(t) = \sum_{i: t_i \leq t} s(t_i) h(t - t_i) : \quad (18)$$

Model (16) belongs to the class of nonlinear self-excited point-processes, in which the nonlinear function is the exponential in our case [Bremaud and Massoulié, 1996; Bremaud et al., 2002]. Bremaud et al. [2002] have given the general condition guaranteeing the existence of a statistically stationary solution in the case of unbounded nonlinear function, sub-exponential distribution of the marks (stress changes  $s$ 's) and long memory kernel as is our case. In our model, the introduction of the integral time scale  $T$  in (13) ensures the existence of the correlation function for any process and for any values of the exponent  $\alpha$ .

#### 4. Derivation of the magnitude dependence of Omori's law

In this section, our goal is to derive Omori's law from model (16) with (12) and (13). The problem can be formulated as follows. Omori's law quantifying the decay of seismic activity after a "mainshock" occurring at the origin of time amounts to determining the typical time dependence of  $\lambda(t)$  conditioned on a value  $M$  realized at  $t = 0$  which is larger than average. This is due to the fact that a mainshock of magnitude  $M$  induces a local burst of seismic activity proportional to  $K 10^M$ , where  $K$  and  $\alpha$  are two positive constants [Helmstetter, 2003]. We note however that previous determinations of the productivity exponent  $\alpha$  have assumed the constancy of  $\alpha$  with mainshock magnitude; in the presence of an exponent  $\alpha(M)$  which increases with  $M$  as we find here, past values of  $\alpha$  have probably been underestimated.

##### 4.1. Theory of Omori's law by generalization of conditional expectations of seismic rates to power law

In the case where averages exist, the Omori law can be expressed in the following general form :

$$E[\lambda(t) | M] = \lambda_{\text{tec}} E[e^{-\lambda(t)} | M] ; \quad (19)$$

where  $E[\cdot]$  denotes the mathematical expectation or average of ensemble of equivalent statistical realizations of the process.

In the case where averages and variances and covariances are ill-defined mathematically, as is the case for Cauchy distributions and for power law with  $\alpha < 2$ , a typical measure of conditional seismicity rate can be defined at any quantile level  $q$  by the probability  $\text{Pr}[\dot{\lambda}(t) > q j_M]$  that the rate  $\dot{\lambda}(t)$  be larger than the quantile  $q$  conditioned on the fact that the seismic rate was at some given value  $j_M$  at time 0:

$$\text{Pr}[\dot{\lambda}(t) > q j_M] = \text{Pr}\left[e^{\dot{\lambda}(t)} > \frac{q}{\tau_{ec}} j_M\right] = \text{Pr}[\dot{\lambda}(t) > (1-\alpha) \ln \frac{q}{\tau_{ec}} j_M] : \quad (20)$$

We are interested in monitoring the time evolution  $q(t)$  of the seismic rate quantile at some probability level  $q$  (which can be varied to explore different fluctuation levels).

If the source terms  $s(t_i)$  were centered Gaussian random variables,  $\dot{\lambda}$  would also be normally distributed. Using (19), this would allow us to obtain

$$E[e^{\dot{\lambda}(t)} j_M] = \exp \left[ E[\dot{\lambda}(t) j_M] + \frac{1}{2} \text{Var}[\dot{\lambda}(t) j_M] \right] ; \quad (21)$$

where

$$E[\dot{\lambda}(t) j_M] = j_M \frac{\text{Cov}[\dot{\lambda}(t); j_M]}{\text{Var}[j_M]} : \quad (22)$$

Using the definition (18), this would provide a closed form expression for the Omori law describing the relaxation of the conditional rate  $E[\dot{\lambda}(t) j_M]$ . The physical meaning of (22) is that one can write a linear regression

$$\dot{\lambda}(t) = \dot{\lambda}_M + \eta ; \quad (23)$$

where  $\dot{\lambda}_M$  is a non-random factor and  $\eta$  is a centered Gaussian noise with zero correlation with  $j_M$ .

Equation (23) writes that the best predictor of  $\dot{\lambda}$  given  $j_M$  is  $\dot{\lambda}_M$ , i.e.,  $E[\dot{\lambda}(t) j_M] = \dot{\lambda}_M$  with

$$\dot{\lambda}_M = \frac{\text{Cov}[\dot{\lambda}(t); j_M]}{\text{Var}[j_M]} ; \quad (24)$$

which retrieves (22).

However, as we explained above, the sources are distributed according to a distribution (12) which can be expected to have a heavy tail, such that both its variance and average are not mathematically

defined, or if they are defined converge very poorly to their asymptotic values even in large data sets. Thus, the standard statistical tools of expectation, variance and covariance can not be used and we need a completely novel approach to tame mathematically these wild fluctuations. For this, we use the insight that the natural generalization of the variance for power laws  $p(x) \propto x^{1-\alpha}$  with infinite variance (i.e., with  $\alpha < 2$ ) is the scale parameter  $C$ , as it possesses most of the properties of the variance for Gaussian random variables: it is additive under convolution of the distribution and it replaces the variance in the expression of the characteristic function of the distribution (see Chap. 4 of [Somette, 2004]).

In the power law case, due to the linear form of (18), we can still write (23) but with  $!_M(t); !_M$  and being power law distributed random variables with the same exponent and with scale factors equal respectively to  $C_!$  (for  $!$  and  $!_M$ ) and  $C$ . The key idea is that can be determined by a generalization of (24), involving generalizations of the covariance and variance. This generalization consists in forming the random variable defined as the product  $!_M = !_M^2 + !_M$ . It is straightforward to show that the distribution of  $!_M$  consists of two main contributions, (i) a dominant power law with exponent  $\alpha = 2$  and scale factor  $C_{!_M} = \alpha^2 C_!$ , and (ii) a sub-dominant power law with exponent  $\alpha$  (with a logarithmic correction) and scale factor  $C_! C$ . This has the following practical implication: if one measures or calculates the leading power law decay of  $!_M$ , the measure of its scale factor gives access to the parameter through the expression

$$\langle !_M(t) \rangle = \frac{C_{!_M}}{C_!} t^{\alpha-2}; \quad (25)$$

where the time dependence of  $\langle !_M(t) \rangle$  comes from that of  $C_{!_M}$  as we show below.

This expression (25) generalizes the standard result (24): notice that the case  $\alpha = 2$  recovers (24) with the correspondence  $C_! = \text{Var}[!]$  and  $C_{!_M} = \text{Cov}[!_M(t); !_M]$ . This is expected since, as we said above, the scale factor reduces to the variance for the Gaussian distribution and the stable Levy law with exponent  $\alpha = 2$  turns out to be nothing but the Gaussian law! We note that this method consisting of generalizing the covariance by introducing the concept of "tail-covariance" has been previously used



to extend the Kalman filter of data assimilation to power law distributed noise processes [Somette and Ide, 2001].

Using (18), we form the product

$$! (t)!_M = \sum_{i,j,t_i,t_j,t_j=0}^X s(t_i) s(t_j) h(t - t_i) h(t - t_j); \quad (26)$$

where the  $s$ 's are random variables with power law tail with exponent  $\gamma$  (specifically, in this paper, the  $s$ 's are Cauchy variables with  $\gamma = 1$  but we give the derivation for any value of  $\gamma$ ). Then, using standard calculations (see Chap. 4 of [Somette, 2004]), the terms in the double sum in (26) that contribute to the leading asymptotic power law tail with exponent  $\gamma = 2$  correspond to the diagonal terms  $s_i = s_j$ , while all the other terms contribute to the sub-leading power law tail with exponent  $\gamma$  with logarithmic corrections. This gives the expression of the scale factor  $C_M^{\gamma=2g}$  of the dominating power law with exponent  $\gamma = 2$

$$C_M^{\gamma=2g} = C_M^{\gamma} \sum_{i,j,t_i=0}^X [h(t - t_i)h(t - t_j)]^{\gamma} : \quad (27)$$

Together with (25), this yields

$$= \theta \sum_{i,j,t_i=0}^X [h(t - t_i)h(t - t_j)]^{\gamma} A^{\gamma} : \quad (28)$$

Since  $h$  is dimensionless,  $A$  is also dimensionless, as it should from its definition (23).

In order to perform a theoretical analysis of (28), it is convenient to transform the discrete sum into a continuous one. Let us consider the times  $t_i$ 's in the sum  $\sum_{i,j,t_i=0}^P$  in (28). Ideally, these times  $t_i$  should themselves be determined self-consistently and are known to follow on average an inverse Omori law. However, such an inverse Omori law is a statistical property observed only for a large ensemble of stacked foreshock sequences while individual sequences exhibit approximately constant seismic rates [Helmstetter and Somette, 2003a]. In order to simplify the analysis, we thus approximate the seismicity prior to a mainshock as being approximately constant in time and uniform in space. This allows us to introduce the average time interval  $\tau$  between two events preceding the mainshock. We expect  $\tau$  to be of the order of the small time-scale cut-off in (13). This is natural if the stress

relaxation is in significant part due to seismicity itself: then,  $c$  is the time scale beyond which the stress relaxation starts to be felt, i.e., when new earthquakes occur in the vicinity of the source. Then, we can approximate the discrete sum as follows:

$$\sum_{i,j,t_i=0}^{\infty} \frac{Z_0}{t} \frac{dt}{t} : \quad (29)$$

Using the form (13) for the stress relaxation kernel gives in continuous time after some manipulations

$$\lambda(t) = \frac{h_0^2}{t^{2\alpha}} \frac{1}{t^{(1+\alpha)-1}} \int_0^{T=t} dx \frac{1}{(x+1+(c=t))^{(1+\alpha)-2}} \frac{1}{(x+(c=t))^{(1+\alpha)-2}} ; \quad (30)$$

where  $h_0 = c^{1+\alpha}$  according to (15). We verify that  $\lambda(t)$  is dimensionless as it should. Under the change of variable  $x \rightarrow y = x + \frac{c}{t}$ , expression (30) can be written

$$\lambda(t) = \frac{h_0^2}{t^{2\alpha}} \frac{1}{t^{2m-1}} \int_{c=t}^{T=\frac{T+c}{t}} dy \frac{1}{(y+1)^m} \frac{1}{y^m} ; \quad (31)$$

where  $m = (1+\alpha) = 2$ .

We now have all the ingredients to estimate (20). We thus obtain

$$\Pr[\lambda(t) > y]_{M} = \Pr[\lambda_M + \dots > y]_{M} = \Pr[\dots > y]_{M} = F(y)_{M} ; \quad (32)$$

where  $F(\cdot)$  is the complementary cumulative distribution of  $\lambda$ . Using (32) in (20), this leads to

$$\Pr[\lambda(t) > q]_{M} = F^{-1}\left(\ln \frac{q}{t_{ec}}\right)_{M} ; \quad (33)$$

The typical time evolution of the seismicity rate  $\lambda(t)$  conditioned on the rate  $\lambda_M$  at time 0 is thus given

by fixing the quantile probability to some level  $\Pr[\lambda(t) > q]_{M} = q$ , leading to

$$\frac{1}{t} \ln \frac{q}{t_{ec}} \lambda(t)_{M} = F^{-1}(q) ; \quad (34)$$

or equivalently

$$\lambda_q(t) = A_q t_{ec} e^{-(t)_{M}} ; \quad (35)$$

where  $A_q = \exp F^{-1}(q)$ . The time-dependence of the seismic decay rate is thus determined by (35),

which requires the determination of the time-dependence of  $\lambda(t)$  given by (30) (and more generally by

(28)).

In the case where the stress relaxation is a pure exponential  $h(t) = e^{-t/T}$ , then using (30), we find  $\dot{\sigma}(t) = e^{-t/T}$  also and the seismic rate  $q(t)$  given by (35) also relaxes exponentially to a constant background. The novel effect that we describe below comes from the interplay between the exponential thermal activation process and the long-memory process of the stress relaxation.

Note that this approach holds also for  $\alpha > 2$  for which variances and covariances exist, which can allow the application of (24). However, using this power approach provides more robust estimators of the typical values of seismic rates when the convergence of the mean and of variances are very slow, as occurs for power laws (see Chap. 3 of [Somette, 2004]).

#### 4.2. Study of the predicted seismicity rate for different values of the two key exponents and

Our purpose is to show that, for a rather broad range of values of the exponents  $\alpha$  and  $\beta$  defining the model,  $q(t)$  is approximately given by

$$q(t) = \frac{1}{t^{\beta(M)}}; \quad (36)$$

with

$$p(M) = a M^\alpha + b; \quad (37)$$

where  $a > 0$  and  $M$  is the mainshock magnitude. In a nutshell, expression (36) with (37) result from the interplay between the heavy-tailed distribution of stress perturbations and the long time memory of the stress relaxation on the one hand and the exponential dependence of the seismic rate on the stress field on the other hand.

##### 4.2.1. Case $\alpha = 1=2$ and $\beta = 2$ (or with a Gaussian distribution of stress source strengths)

This interplay between the long time memory of the stress relaxation and the exponential dependence of the seismic rate on the stress field is exemplified by the case  $\alpha = 1=2$  and  $\beta = 2$ , which has previously been shown to give exact multifractal properties in the time domain [Muzy and Bacry,

2002], and as a consequence continuous dependence of the relaxation exponents  $p(M)$  as a function of shock magnitudes  $M$ . This continuous dependence of the exponent  $p(M)$  has actually been documented empirically in this case in another context of aftershock decay following shocks in financial markets [Somette et al., 2003]. Schmitt [2003] has studied in details the properties of the process (17) with (18), when  $s(t)$  is a Gaussian white noise (corresponding formally to  $\alpha = 2$ ), with the memory exponent  $\alpha = 1/2$ .

An intuitive grasp of this behavior is obtained by examining  $d = dt$ :

$$\frac{d}{dt} = \frac{(h_0^2 - t^{2\alpha})}{t} - \frac{(T + c)^{1-\alpha}}{(T + c - t)^{1-\alpha}} - \frac{c^{1-\alpha}}{(t + c)^{1-\alpha}} : \quad (38)$$

It is easy to see that the first (resp. second) term of the bracket in the r.h.s. is always larger (resp. smaller) than 1, which ensures that  $\frac{d}{dt}$  is always negative. In addition, for  $t < T$ , the bracket in the r.h.s. is almost constant and close to 1, showing that  $d = dt \approx 1 - t$  and thus  $\ln(t) \approx \ln(T) - (1 - t)$ . Then expression (35) leads to (36,37) using the fact that  $\ln(M) / \ln(K \cdot 10^M) = \ln 10 M + \ln K$ , i.e.,  $\ln(M)$  is linearly related to the magnitude  $M$ . Here, we have used the productivity law that an earthquake of magnitude  $M$  produces on average a number of aftershocks proportional to the exponential of its magnitude ( $\alpha$  is the productivity exponent often reported between 0.5 and 1).

#### 4.2.2. Condition $2m = (1 + \alpha) = 1$

This case corresponds to taking the exponent  $m = (1 + \alpha) = 2$  defined in (31) equal to  $1/2$ . Then,  $\frac{d}{dt} \approx 1 - t$  has exactly the expression given by the right-hand-side of (38), showing that  $\frac{d}{dt} \approx 1 - t$  is close to  $1 - t$ , and thus  $\ln(t) \approx \ln(T) - (1 - t)$  which, for not too small nor too large  $t$ 's and for  $\text{constant}_1 < \text{constant}_2$ , gives  $\ln(t) \approx \ln(T) - (1 - t)$ . This yields (36,37). Typically, the power law behavior is observed over more than two decades in time, which is comparable to empirical observations. Figure 1 shows the numerical evaluation of  $\ln(t)$  as a function of  $\ln(t=T)$  for several pairs  $(\alpha; \beta)$  which obey the condition  $(1 + \alpha) = 1$  exactly:  $(\alpha = 3; \beta = 2/3); (\alpha = 2; \beta = 0.5); (\alpha = 1; \beta = 0); (\alpha = 2/3; \beta = 0.5); (\alpha = 0.5; \beta = 1)$ , using

$c=T = 10^{-6}$ . We verify the existence of a linear decay of  $\dot{\rho}(t)$  in the variable  $\ln t$ , which qualifies an Omori power law (36). The range of this Omori power law regime depends rather sensitively on the temperature, on the mainshock magnitude and on the ratio  $c=T$  since the logarithm of the seismic rate is proportional to  $\ln t$  via a coefficient of proportionality involving the inverse temperature and the mainshock magnitude, as shown in (35). Then, by the same argument as in section 4.2.1, the linear dependence of  $\dot{\rho}_M$  on  $M$  in expression (35) leads to (36,37).

The fact that  $\dot{\rho}(t)$  is asymptotically exactly logarithmic in time for  $2m = (1 + \alpha) = 1$  and thus that the seismic rate  $\dot{\rho}(t)$  is an Omori power law can be recovered from a different construction motivated by multiplicative cascades introduced in turbulence. The discrete multiplicative cascade model of hydrodynamic turbulence can be extended in distribution to the continuous limit [Schmitt and Marsan, 2001] and shown to take the form (18) expressed with the discrete sum replaced by a continuous integral. Then, Schmitt and Marsan [2001] show that the only condition for exp[ $\cdot$ ] (in our case through (17)) to be "logstable multifractal" is that the exponent  $\alpha$  of the distribution of the innovations  $s$  and the exponent  $1 + \beta$  of the memory kernel be related by the condition  $(1 + \beta) = 1$  that we have derived above through a different route. In a nutshell, their argument (which applies in distribution to one-point statistics but not to multipoint statistics nor in process) is as follows. The logarithm of  $\dot{\rho}$  is constructed as an integral in the time-scale  $(t;a)$  domain within a cone with apex on the time axis of identically independent distributed innovations distributed according to a Levy distribution with exponent  $\alpha$ . The natural scale-invariant measure for this integral in this time-scale domain is  $da dt = a^{-2}$  in the sense that it is (left-)invariant by the translation-dilation group [Muzy and Bacri, 2002]. The contribution of a vertical strip of width  $dt = \delta t$  centered at time  $t$  (i.e., at a distance  $\delta t$  from the present time  $t$ ) within the cone is  $\int_t^{t+\delta t} da a^{-2} = \delta t^{-1} (\psi(t) - \psi(t - \delta t))$ , where  $\psi$  is a Levy distributed noise with scale factor unity. The exponent  $1 - \alpha$  comes from the dependence of the scale factor of sum of the  $\psi(t)$  Levy variables that contribute to each trip. Now, in distribution, the total integral is thus equal to the sum of all strips up to time  $t$ , which gives  $\int_0^t d\tau \delta \tau^{-1} (\psi(t) - \psi(t - \delta \tau))$ . This expression is exactly of the form (18) with  $1 + \beta = 1 - \alpha$ . QED.

#### 4.2.3. Case $2m = (1 + \epsilon) \notin 1$

It is useful to study the generalization of (38), which reads

$$\frac{d[t^{2m-1-\epsilon}]}{dt} = \frac{(h_0^2 - t^2)}{t^{2-m}} - \frac{(T+c)^{1-(m=2)}}{(T+c-t)^{m=2}} - \frac{c^{1-(m=2)}}{(t+c)^{m=2}} : \quad (39)$$

Two cases must be distinguished.

For  $2m = (1 + \epsilon) < 1$ , the first (resp. second) term of the bracket in the r.h.s. of (39) is always larger (resp. smaller) than 1, which ensures that  $\frac{d[t^{2m-1-\epsilon}]}{dt}$  is always negative. In addition, for  $t < T$ , the bracket in the r.h.s. is almost constant and close to  $(T+c)^{1-m}$ , showing that  $d[t^{2m-1-\epsilon}]/dt \approx -t^{1-2m}$  and thus  $t^{2m-1-\epsilon}(t) = \text{constant}_1 - (T+t)^{2m-1-\epsilon} + \text{constant}_2 - (T+t)^m$ . is thus a convex decreasing function of  $\ln t$  (with a upward curvature) as shown in figure 2. The mathematical form of the decay rate tends to slow down compared with a standard Omori power law. This convexity tends to linearity as  $m \rightarrow 1/2$ .

For  $2m = (1 + \epsilon) > 1$ , we have  $1 - (m=2) < m=2$ . As a consequence, for small  $t$ 's,  $(T+c-t)^{m=2} > (T+c)^{1-(m=2)}$  while the reverse inequality holds true for large  $t$ 's. This reasoning shows that the bracket is negative for small  $t$ 's and becomes positive for large  $t$ 's. Therefore,  $\frac{d[t^{2m-1-\epsilon}]}{dt}$  is positive for small  $t$ 's, vanishes at an intermediate time and becomes negative for large  $t$ 's. This translates into increasing for small  $t$ 's, passing through a maximum before decreasing for large  $t$ 's, as shown in figure 2. In this case, we can often observe an approximate linear decay of  $t(t)$  as a function of  $\ln t$ , over two to three order of magnitudes in time in the decaying part beyond the maximum, all the more so, the closer  $m$  is to one. Over this range, by the same argument as in section 4.2.1, the linear dependence of  $\log M$  on  $M$  in expression (35) leads to (36,37).

## 5. Empirical investigation of Omori's law conditioned on main shock magnitudes

### 5.1. Data selection and analysis of completeness

We use the Southern Californian earthquakes catalog with revised magnitudes (available from the Southern California Earthquake Center) as it is among the best available in terms of quality and time span. Magnitudes  $M_L$  are given with a resolution of 0.1 from 1932 to 2003, in a region from approximately 32° to 37° N in latitude, and from 114° to 122° in longitude.

Using all the data of this catalog, we compute the complementary cumulative magnitude distribution for each year from 1932 to 2003 included. This gives 72 Gutenberg-Richter distributions which are shown in Figure 3. The logarithms of the distributions as a function of magnitude are approximately linear for the largest magnitudes and exhibit a cross-over to a plateau at small magnitudes. In order for our analysis to be robust, we need to address the question of completeness of the catalog. The level of low-magnitude plateau increases with time, which is the consequence of the evolution of the seismic network: as more stations are added, the spatial coverage increases, so that the number of events with fixed magnitude also increases. One can also observe that events of smaller and smaller magnitudes are detected and located when going from 1932 to the present. This also leads to an increase of the number of events recorded in the catalog. As the typical time scale over which we analyze the Omori law decay is about 1 year, which is small compared with the average time scale of the evolution of the network coverage (see Figure 3), we will consider all events in the catalog that have a magnitude that belong to the linear part of the magnitude distribution curve. Figure 4) shows several complementary cumulative distributions of earthquake magnitudes for the four years 1932, 1975, 1992 and 1994. Taking the linear relationship between the logarithm of the distribution as a function of magnitude as the standard criterion for completeness [Kagan, 2003], we infer that the catalog is approximately complete for  $M_L > 3$  in 1932 and later years, for  $M_L > 2.5$  in 1975 and later years, for  $M_L > 2$  for 1992 and later years, and for  $M_L > 1.5$  in 1994 and later years. Since our tests of

aftershock decay rate are performed typically over a time range starting beyond one day and extending to several hundred days, the short-term lack of completeness identified by Kagan [2004] is not an issue here. Actually, the problem of the short-term completeness of aftershock catalogues is the most acute for large mainshocks [Kagan, 2004], which allows us to extend the study of the seismic decay rate at shorter times for the small mainshock magnitudes.

In order to maximize the size of the data used for our analysis (to improve the statistical significance) and to test for the stability of our inversion, we will consider four different sub-catalogs:

1. 1932 – 2003 for  $M_L > 3$  (17;934 events),
2. 1975 – 2003 for  $M_L > 2.5$  (36;614 events),
3. 1992 – 2003 for  $M_L > 2$  (54;990 events), and
4. 1994 – 2003 for  $M_L > 1.5$  (86;228 events).

The fact that the number of events in these sub-catalogs increases as their time-span decreases is due to the lowering of the minimum magnitude of completeness which more than compensates the reducing time interval.

## 5.2. Construction of the time series of aftershocks

### 5.2.1. Time-shifted stacked sequences: general principle

We now describe the method used to determine the validity of the Omori law and to measure the p-value as a function of the mainshock magnitude.

We consider all events in a given sub-catalog and discriminate between mainshocks and triggered events ("aftershocks"). Mainshocks are determined by using declustering methods which are described below in sections 5.2.2 and 5.2.3: to test for the robustness of our results and their lack of sensitivity with respect to the specific choice of a declustering method, we present two different implementations.



Once the mainshocks are determined, triggered events are defined as those events following a mainshock, which belong to a certain space-time neighborhood of it. This space-time neighborhood is specified below. We thus have as many triggered ("aftershock") sequences as there are mainshocks.

In order to test for the predicted dependence of the  $p$ -value as a function of magnitude, we need to bin the mainshock magnitudes in intervals  $[M_1; M_2]$ . We have chosen the intervals (when available)  $[1.5; 2]$ ,  $[2; 2.5]$ ,  $[2.5; 3]$ , and so on up to  $[7; 7.5]$ .

In each mainshock magnitude interval  $[M_1; M_2]$ , we consider all triggered sequences emanating from mainshocks with magnitude in this interval  $[M_1; M_2]$ . We translate each triggered sequence so that their origin of time (their mainshock time) is moved to the common value  $t = 0$ . Then, we stack all these sequences to obtain a mega-sequence containing all triggered events coming from mainshocks in the same magnitude interval  $[M_1; M_2]$ .

We then bin the time axis according to a geometrical series, and estimate the average rate of events within each bin. The resulting function is fitted using the modified Omori law

$$N(t) = B + \frac{a}{(t + c)^p}; \quad (40)$$

where  $B$  is a positive parameter introduced to account for the background seismicity assumed to be superimposed over the genuine triggered sequences. The time shift  $c$  ensures the regularization of the seismic rate at  $t = 0$ .

Varying  $[M_1; M_2]$  allows us to test for a possible dependence of  $p$  as a function of the magnitude of the mainshock. In order to (i) maximize the size of the data sets, (ii) avoid bias due to incompleteness of the catalogs, and (iii) test the robustness of our conclusions, we will use

1. for  $M_1 = 3$ : four different sub-catalogs (1932–2003, 1975–2003, 1992–2003, 1994–2003), giving four estimates for the  $p$ -value;

2. for  $M_1 = 2.5; M_2 = 3$ : three sub-catalogs covering 1975–2003, 1992–2003 and 1994–2003, giving three estimates for the p-value;
3. For  $M_1 = 2; M_2 = 2.5$ : two sub-catalogs covering 1992–2003 and 1994–2003, giving two estimates for the p-value;
4. For  $M_1 = 1.5; M_2 = 2$ : one sub-catalog covering 1994–2003, giving a single estimate for the p-value.

To explore further for the robustness of our estimates for  $p$ , we will also impose  $c = 0$  to test for the sensitivity with respect to the beginning of the stacked time series. We will also remove bins at random and re-estimate the p-values of these pruned stacked sequences. Putting all these estimates together for a given magnitude interval  $[M_1; M_2]$  allows us to obtain a mean value and a standard deviation. Note that for each magnitude interval, we have several thousand events in the decay rate function, ensuring an adequate estimation of the p-value. For large magnitudes, there are only a few mainshocks contributing to the stacked sequence, but each of them have numerous aftershocks. For small magnitudes, each mainshock contributes few triggered events (some have none) but, due to their large number, the stacked sequences have also a sufficiently large number of events, even for the smallest magnitude intervals.

We now present the two declustering methods that we have implemented to select the mainshocks.

### 5.2.2. 1st declustering technique

The first method is essentially the same as defined in [Helmstetter, 2003]. First, every event in the catalog is defined as a mainshock if it has not been preceded by an event with larger magnitude within a fixed space-time window  $T \times d$ , with  $T = 1$  year and  $d = 50$  km. Looking for events triggered by this mainshock, we define another space-time window following it. The time dimension of the window is also set to 1 year, whereas the space dimension depends on the rupture length of the main event. This

spatial window is chosen as a circle of radius equal to the mainshock rupture length

$$L = 10^{2.57 + 0.6M_L}; \quad (41)$$

which is the average relationship between  $L$  and magnitude  $M_L$  for California [Wells and Coppersmith, 1994]. If any event falls within this space-time window, it is considered as triggered by the main event. Note that, since the reported uncertainty of events localization is about 5km, we set the size of the spatial window to 5km if  $L < 5\text{km}$ . We have also checked the stability of the results by considering a spatial neighborhood of radius  $2L$  rather than  $L$  for the triggered events.

### 5.2.3. Second declustering technique

The second declustering technique is the same as the first one, except for one element: the space window used for qualifying a mainshock is not fixed to  $d = 50\text{km}$  but is chosen to adapt to the size of the rupture lengths  $L(M_i)$  given by (41) of all events of all possible magnitudes  $M_L(i)$  preceding this potential mainshock. In other words, a potential mainshock is selected if there are not preceding events within one year in its past, which are at a distance less than twice their own rupture length. The space-time window for the selection of triggered events is the same as for the first declustering method.

This second procedure of declustering is perhaps more natural than the first one, especially for small magnitude events. To take an extreme example, in the first method, an event of magnitude 1.5 can not be selected as a main event if it falls within 50km of a previous larger event, even if the rupture length of the latter is much smaller than 50km. This obviously prevents almost all events of magnitude 1.5 to be considered as mainshocks, and thus biases the statistics. Mainshocks of low magnitudes which are selected by the first declustering method will on average occur within areas of very low seismicity rate, so that the composite triggered sequence will be under-representative. Moreover, all events located at say 51km of an event of magnitude  $M_L = 7.5$  are defined as main events, whereas they probably belong to its triggered sequence. We can thus expect the first declustering technique to penalize heavily the quality of the stacked sequence associated with mainshocks of low magnitudes.

The second declustering technique do not show such biases.

### 5.3. Results

#### 5.3.1. Least-square fit of the seismic rate as a function of time with equation (40)

Figures 5-8 show sets of typical seismic decay rates of stacked sequences for several magnitude intervals of the mainshocks. Only half of the individual Omori curves are drawn for the sake of clarity, as in all similar figures in the remaining of the paper. Figure 5 (respectively Figure 6) corresponds to the period from 1932 to 2003 when using the first (respectively second) declustering technique, with mainshock magnitudes above  $M_L = 3$ . Figure 7 (respectively Figure 8) corresponds to the period from 1994 to 2003 when using the first (respectively second) declustering technique, with mainshock magnitudes above  $M_L = 1.5$ . Very similar plots are obtained for different time periods and by varying the size from  $L$  to  $2L$  of the spatial domain over which the triggered sequences are selected. For large mainshock magnitudes, the roll-off at small times is due to the observational saturation and short-time lack of completeness of triggered sequences [Kagan, 2004]. In some cases, one can also observe the cross-over to the constant background at large times.

Figure 9 shows the fitted p-values as a function of the magnitude of the mainshocks for each of the four sub-catalogs (the abscissa corresponds to the magnitude  $(M_1 + M_2)/2$  in the middle of the range  $[M_1; M_2]$  for each interval). We use a standard least-square fit of the seismic rate as a function of time with a weight proportional to  $t$  for each bin to balance their relative importance. We take into account the possible presence of a background term as shown in equation (40).

Figure 10 plots the average p-values and their error bars as defined above. Both figures exhibit a very clear increase of the p-value with the mainshock magnitude. For magnitudes  $M_L \geq 3$ , a linear fit

$$p(M_L) = 0.12M_L + 0.28 \quad (42)$$

is shown as the straight line in Figure 10. The deviation from this linear behavior for the lowest magnitudes  $M_L \leq 2.5$  can be attributed to the biases associated with the first declustering technique, as explained above, when comparing with the results of the second declustering method.

Figure 11 shows the p-value and its standard deviation as a function of mainshock magnitude

obtained with the second declustering method. As with the first declustering method, this data is well-fitted by a linear relationship

$$p(M_L) = 0.10M + 0.37 : \quad (43)$$

#### 5.4. Maximum Likelihood Estimation method

In order to check the reliability of the  $p$ -values obtained in the previous analysis, we also used a maximum likelihood estimation (MLE). We obtain the MLE of the  $p$ -value in a finite time window from  $t$  to  $t_U$ , by maximizing the probability that the particular temporal distribution of the  $N$  events in that window results from Omori's law with this particular  $p$  value. The most likely  $p$  value is then given by the implicit equation [Huang et al., 2000]

$$\frac{1}{p-1} + \frac{t_U^{p-1} \ln t - t^{p-1} \ln t_U}{t_U^{p-1} - t^{p-1}} = \ln t_N ; \quad (44)$$

where the  $t_n$  are the time occurrences of the  $N$  events between  $t$  and  $t_U$  and

$$\ln t_N = \frac{1}{N} \sum_{n=1}^N \ln t_n : \quad (45)$$

We fixed  $t_U = 1$  year, while  $t$  was varied continuously from  $10^{-4}$  to 0.5 year and we solve for  $p$  in the implicit equation (44). We could thus check both the value and the stability of  $p$  with sample size and to time boundary effects.

Figure 12 shows  $p$  as a function of  $t$  for the post-1932 sub-catalog, using the first declustering technique, with  $R = 2L$ , for different magnitude ranges. This figure should be compared with Figure 5. One can observe that, for  $3 < M < 3.5$ ,  $p$  varies very slightly with time  $t$ , with a value of about 0.6, whereas the least-square fit gave  $p = 0.67$  for the whole time range (corresponding here to  $t = 10^{-4}$  year). For  $4 < M < 4.5$ ,  $p$  is close to 0.9, while the least-square fit gave  $p = 0.85$ . The case  $5 < M < 5.5$  is different as the maximum likelihood yields a  $p$ -value of about 0.85 whereas the least-square fit gave  $p = 0.96$ . It should be noted here that the least-square fit detected a significant non-zero background value  $B$ , and that the MLE method doesn't take into account such a term, which leads to an underestimation of  $p$  as the time-distribution is flatter at larger times (which is also expressed by a

strong drop of  $p$  at large time  $t$ ). The case  $6 < M < 6.5$  yields  $p$  close to 0.8 whereas the least-square  $t$  gave  $p = 1.29$ , but the MLE method also takes account of events for times larger than 0.1, where strong secondary aftershock activity disturbs the distribution and would tend to define a power-law with lower exponent. Considering the  $7 < M < 7.5$  range, where no such bias occurs, the MLE method gives  $p$  very close to 1 for  $10^{-3} < t < 10^{-2}$  whereas  $p = 0.99$  for the least-square  $t$ . The conclusion is thus that, when a background  $B$  is absent,  $p$ -values obtained with both methods agree very well, which strenghtens our belief in the reliability of the exponents determined with the least-square  $t$ . This least-square  $t$  has here the advantage that it takes into account the possible existence of a non-zero background term  $B$ .

Using the same data set and the 2nd declustering method, we obtained Figure 13, which can be compared to Figure 6. Once again, exponents agree very well (except for the  $6 < M < 6.5$  range, for reasons explained above).

We also check the consistency of both methods for the post-1994 catalog. The MLE provided us Figure 14 for the first declustering method, which has to be compared with Figure 7. We note that  $p$ -values perfectly agree up to range  $3.5 < M < 4$ . For the next magnitude range, the MLE provides a  $p$ -value that is continuously decreasing with  $t$ . This can be rationalized by a look at the least-square  $t$ , which shows that the distribution converges toward a constant background rate at large times, so that the ML inversion is systematically biased towards low values. The  $5.5 < M < 6$  gives  $p$  close to 0.9 compared with 1.07 with the least-square  $t$ . Once again, the existence of non-zero background term certainly biases the MLE. The last magnitude range,  $6.5 < M < 7$  offers the largest discrepancy between  $p$ -values, but it should be noted that for times larger than 0.01 year, the  $p$ -value varies between 1.15 and 0.8, so that the average maximum likelihood value agrees well with the least-square inversion. Even in the worst case ( $t = 10^{-2}$  year), the MLE method even emphasises the variation of  $p$  with magnitude.

The results for the 2nd declustering technique on the same sub-catalog are displayed in Figure 15 (which should be compared with Figure 8). The  $p$ -value for the lowest magnitude ranges are quite low

(0.2-0.3) but this is once again due to the background rate. The value obtained in the  $3.5 < M < 4$  range (p around 0.7) is strongly oscillating. This is indeed also the case for the time distribution shown in Figure 8, for which  $p = 0.57$ . Note that the MLE method yields  $p = 0.65$  for  $t = 10^{-4}$ , close to the least-square  $t$  value obtained on the same data range. We have the same comments as above for the  $4.5 < M < 5$  which displays a noticeable background term. The next magnitude range gives a p-value a bit less than 0.9, whereas the least-square  $t$  gave  $p = 0.85$ . The same comments as above apply for the  $6.5 < M < 7$ .

Overall, the conclusion is that, when the background rate is absent from the seismic decay, p-values inverted from both methods agree very well, and that even when we observe a discrepancy, the ML inversion amplifies the variation of p with magnitude.

#### 5.5. Tests of our procedure with synthetic ETAS catalogs

To test the reliability and robustness of our results, we now analyze simulated catalogs with known statistical properties following exactly the same procedure as for the real catalogs. We generated synthetic catalogs using the ETAS model, running the code of K. Feltzer and Y. Gu (spring 2001) modified by A. Helmstetter (2003). This model has a fixed magnitude-independent Omori-p-value as an input. Thus, by construction, synthetic catalogs generated with the ETAS model should exhibit Omori laws with magnitude-independent exponents. Applying our procedure to such synthetic catalogs, which are known to be very similar to real catalogs in many of their statistical properties [Helmstetter and Sornette, 2003], allows us to investigate whether the magnitude-dependence of the p-value reported above could result from some bias introduced by our analysis rather than being a genuine property of earthquake catalogs.

In the ETAS model, a main event of magnitude  $M$  triggers its own primary aftershocks according to the following distribution in time and space

$$n_m(r;t) dr dt = K 10^{(M - M_0)} \frac{c dt}{(t + c)^{1+\alpha}} \frac{d dr}{(r + d)^{1+\beta}} ; \quad (46)$$

where  $r$  is the spatial distance to the main event (considered as a point process). The spatial

regularization distance  $d$  accounts for the finite rupture size. The power law kernel in space with exponent  $\beta$  (this exponent should not be confused with that of the distribution of the stress fluctuations defined in (12)) quantifies the fact that the distribution of distances between pairs of events is well described by a power-law [Kagan and Jackson, 1998]. In addition, the magnitude of these primary aftershocks is assumed to be distributed according to the Gutenberg-Richter law of parameter  $b$ . The ETAS model assumes that each primary aftershock may trigger its own aftershocks (secondary events) according to the same law, the secondary aftershocks themselves may trigger tertiary aftershocks and so on, creating a cascade process. The exponent  $1 + \beta$  is not the observable Omori exponent  $p$  but defines the local (or direct) Omori law [Somette and Somette, 1999; Helmstetter and Somette, 2002a]. The two exponents  $b$  and  $\beta$  should not be confused with those used for the Green function of viscous relaxation.

Using the ETAS code, we thus generated a catalog of earthquakes located within a three-dimensional slab of horizontal dimension  $500 \times 500 \text{ km}^2$  and thickness  $20 \text{ km}$ . We added a noise with amplitude of  $5 \text{ km}$  to the position of each event to simulate the location uncertainty of real catalogs. The parameters of the ETAS model were chosen as follows:  $b = 0.9$ ,  $\beta = 1.1$ ,  $c = 10^{-5} \text{ day}$ ,  $K = 0.002$ , and  $\alpha = b = 0.9$ . The characteristic spatial distance  $d$  in the ETAS kernel was taken equal to the event rupture length (which we deduced from its magnitude, according to the Wells and Coppersmith (1994) relationship (41)), while the spatial decay exponent was fixed to  $1.0$ . The minimum magnitude of generated events was set to  $M_0 = 0.5$ , and we introduced a truncation of the Gutenberg-Richter distribution such that no event of magnitude  $M_1 > 8.0$  are allowed. The rate of background events was set to  $50 \text{ events/day}$ . The obtained synthetic catalog is 25 years long, and only the 10 last years are retained to minimize temporal edge effects at the beginning of the time-series. Finally, only events of magnitude larger than  $1.5$  were kept in the catalog, to mimic the effect of a magnitude detection threshold of real seismic networks. We performed several simulations until we generated a catalog similar to the post-1994 sub-catalog we previously analyzed: by similar, we mean that the synthetic catalog has approximately the same total number of events and the same number of events with magnitude  $M_1 > 7.0$ . With these parameters, the branching ratio (mean number of triggered events per shock) is  $n = 0.983$  and the characteristic



time  $t$  below which the bare Omori law  $1=t^{-1}$  is renormalized into the observable global Omori law  $1=t^{-1}$  is  $t = 1:1 \cdot 10^4$  years. Thus, the p-value of any aftershock sequence is by construction equal to  $p = 1 - 0.9 = 0.1$  in the time interval  $[10^4 \text{ year}, 1 \text{ year}]$  that we used for our analysis, which is the same time scale used for our analysis of aftershock sequences of real catalogs.

The selection of mainshocks and aftershocks in our synthetic catalog was performed using the second declustering algorithm (with  $R = 2L$ ) described in section 5.2.3, and we used the same stacking method to derive empirically the  $p(M_1)$  relationship. The results obtained with the fits of the logarithm of the stacked seismic rates as a function of the logarithm of time are shown in Figure 16. The p-values are found independent of the magnitude of the mainshock and close to the correct value. There is actually a tendency for the p-value to decrease with the mainshock magnitude (which is the opposite of the effect predicted by our model and reported for the real catalogs). The origin of this effect is the following: for mainshocks of small magnitudes, there are so many stacked time-series that fluctuations average out allowing to retrieve a precise p-value; in contrast, after mainshocks of large magnitudes, strong secondary aftershock sequences often occur which introduce large fluctuations. As there are only a few stacked aftershock series associated with the relatively rare large mainshocks, the fluctuations of the average seismic rates after the large mainshocks do not average out; bursts of strong aftershocks tend to bias the p downward leading to its under-estimation. To minimize this effect for events of large magnitudes, we fitted the Omori law over the beginning part of the time series and removed the end of the time-series to compute p (see Figure 16).

We also inverted p on the same synthetic data using the maximum likelihood formula (44) in a finite time window from  $t$  to  $t_f$ , following the same method as for the real catalogs. We span  $t$  up to  $t_f = 2$ . Figure 17 plots the p-value in different mainshock magnitude ranges as a function of  $t$ . Since the MLE method is sensitive to the background seismicity, using the lessons from our previous analysis on the real catalogs, we restricted  $t_f$  to avoid biases due to the background seismicity. Thus, for magnitudes up to 3, we did not take into account data for times larger than 0.01 year. This upper cut-off has been set to 0.1 year for the 3.5 - 4 magnitude range, and no cut-off (that is,  $t = 1$  year)

was imposed for larger magnitude ranges since their larger triggered seismicity makes the background negligible up to one year after the mainshocks. The results are not sensitive to these specific cut-offs as long as they correspond to negligible background seismicities. Figure 17 clearly shows that the  $p$ -values cluster around  $p = 0.9$  whatever the magnitude range. Oscillations occurring at large times correlate with oscillations observed on the binned data, and betray the influence of secondary aftershock sequences.

These results and the accuracy of the recovered  $p$ -values in our synthetic catalog strengthen one's confidence in our reported results that the magnitude dependence of the  $p$ -value in the real Southern California catalogs is a genuine effect and not an artifact of our data analyzing procedure.

## 6. Discussion

### 6.1. Summary

We have proposed a new physically-based "multifractal stress activation" model of earthquake interaction and triggering based on two simple ingredients: (i) seismic ruptures result from activated processes giving an exponential dependence of the seismic rate on the local stress; (ii) the stress relaxation has a long memory, typically larger than one year. The combination of these two effects gives rise in a rather general way to seismic decay rates following mainshocks that can be well-described by apparent Omori laws with exponents  $p$  which are linearly increasing with the magnitude  $M_L$  of the mainshock. This  $p(M_L)$  dependence can be interpreted as a temporal multifractality, that is, as a continuous spectrum of exponents, each exponent being associated with a given singularity strength (mainshock magnitude).

While rather general, these predictions require, within our model, that the two exponents (stress relaxation) and (stress strength distribution) verify approximately the condition  $(1 + \alpha) = 1$ . We stress that the special case ( $\alpha = 2$ ;  $\beta = 1/2$ ), which has been shown to give an exact multifractal process, obeys this condition. Since  $\alpha$  and  $\beta$  are two inputs, our theory is mute on the possible origin

of this condition. The fact that such a constraint appears as the condition to observe an Omori power law is a very interesting prediction to test in the future. As a bonus, this condition predicts the multifractality expressed by a dependence of the Omori exponent on the earthquake magnitude. These results can also be seen to provide a generalization to the multifractal random walk ( $\alpha = 2$ ;  $\beta = 1/2$ ) of Muzy and Bacry, 2002; Schmitt and Marsan, 2001], by showing that multifractality is not an isolated property at a single point in the plane ( $\alpha$ ;  $\beta$ ) but occurs over a line of co-dimension 1. At this stage, we can only conjecture that a broader model embodying the self-organization of the stress field and earthquake space-time organization will lead to the prediction that indeed the two exponents  $\alpha$  and  $\beta$  are not independent but are linked by the condition  $(1 + \beta) = \alpha$ .

These predictions have been tested by a careful and detailed analysis of earthquake sequences in the Southern California Earthquake catalog. The robustness of the results obtained with respect to different time intervals, magnitude ranges, declustering methods suggests that we have discovered a new important fact of seismicity: the apparent power law relaxation of seismic sequences triggered by mainshocks has indeed an exponent  $p$  increasing with the mainshock magnitude by approximately 0.1–0.15 unit for each magnitude unit increase. The fits (42) and (43) of the data are in agreement with the theoretical prediction (37) of the proposed multifractal stress activation model.

## 6.2. Intuitive “proof” that $p(M_L)$ increases with $M_L$ for any multifractal generalization of Omori’s law

Here, we give an heuristic and intuitive reason why, if  $p$  varies with  $M_L$ , this can only be by increasing with the mainshock magnitude.

Consider the plate tectonic process which continuously produces earthquakes, which trigger other earthquakes and so on, with a productivity increasing with the earthquake magnitude. Let us study the temporal evolution in a fixed spatial domain. This temporal evolution can be viewed to define a statistically stationary measure defined on the temporal axis, the measure determining the rate of earthquakes at any possible instant. A general method for quantifying such measure is to calculate its

multifractal spectrum. For instance, if the seismic rate is constant, the measure is uniform and the multifractal spectrum is reduced to a point of dimension  $f(\alpha) = 1$  at the singularity strength  $\alpha = 1$ . Note that this notation refers in the present discussion to the exponent of a local singularity and not to the exponent of the productivity law.

An Omori sequence with exponent  $p$  corresponds to a singularity (to the right) equal to  $1 - p$  (for  $p \neq 1$ ). Let us calculate the singularity spectrum of the seismic rate measure. This is usually done via the calculation of moments of order  $q$ , large positive  $q$ 's corresponding to small  $\alpha$ 's, that is, to strong singularities (see for instance Chapter 5.2 in [Somette, 2004]). Now, a large earthquake triggers a strong burst of seismicity, giving rise to a strong singularity. From the relation  $\alpha = 1 - p$ , to be consistent with the multifractal description, a large earthquake must be associated with a strong singularity, a small  $\alpha$ , hence a large  $p$ . Reciprocally, small moment orders  $q$  select weak seismic sequences, which are thus associated with small local mainshocks. Small  $q$ 's are associated with large  $\alpha$ 's, hence small  $p$ 's. Thus, any generalization that allows for a dependence of  $p$  on the mainshock magnitude necessarily leads to an exponent  $p$  increasing with the magnitude.

By a similar argument in the space domain, the exponent of the spatial decay of the seismic rate induced by a mainshock of magnitude  $M_L$  should increase with  $M_L$ . Thus, in this view, the ETAS model is nothing but the mono-fractal approximation of the more general multifractal description of seismicity.

### 6.3. Self-similarity of earthquakes

A central empirical observation in seismology is the inability to discriminate between rupture processes of large and small earthquakes. The signature of this self-similarity of individual seismic events translates into the invariance of the stress drop (inverted from seismic waves) with rupture size. It would thus seem that Figure 9 for instance is contradicting this empirical law since the statistics of the time-series of triggered events depend on the mainshock magnitude. This could be interpreted as reflecting different rupture mechanisms, thus breaking scale invariance. However, such an interpretation

is incorrect. First, it is now well-understood that mono-fractality embodied in a universal (Omori) power law is not the only signature of scale invariance. Since Parisi and Frisch [1985] and Halsey et al. [1986], several complex systems have been shown to exhibit an extended form of scale invariance, called multifractality. The  $p(M)$  dependence documented here is an example of such multifractality. Second, the main ingredients of our theoretical model are scale invariant: (i) the triggering mechanism of a single shock is stress activation, independently of the magnitude of the event to be nucleated; (ii) we make no assumption the stress drop during an event; (iii) the Cauchy law (11) (exponent  $= 1$  in (12)) was suggested by Kagan [1994] using the self-similarity argument, and our theoretical results show that even in that case  $p$  depends on  $M$ . Once again, the long memory of the stress relaxation kernel coupled with the exponential stress activation are sufficient to predict such a magnitude dependence, which is thus compatible with the self-similarity hypothesis.

#### 6.4. Alternative models

Could these observations be interpreted differently than with the multifractal stress activation model? For instance, a change of the apparent Omori exponent  $p$  is consistent with the ETAS model if the critical branching ratio  $n$  (average number of triggered events per main shock) is less than unity: if  $n$  is close to its critical value 1,  $p$  is close to 1, while for  $n < 1$ ,  $p$  goes from 1 at short time scale to  $1 + \frac{1-n}{n}$  beyond a characteristic time scale  $t_c = (1-n)^{-1}$  [Somette and Somette, 1999; Helmstetter and Somette, 2002a]. The parameter  $n$  is often found in the range 0.2–0.3 for large shocks. Thus, to explain our results (42) and (43), one would need to invoke a larger value for  $n$  of the order of 0.5 and to have  $n$  depend on main shock magnitudes. Or if the measurement for small main shock magnitudes are performed at shorter times than for larger main shocks, this would lead to an increase of the  $p$ -value because short times should be controlled by the exponent 1 while longer time reveal the exponent  $1 + \frac{1-n}{n}$ . However, this last explanation is ruled out by the fact that our determination of the  $p$ -values is performed on the same time interval for all magnitudes.

One could also perhaps argue that small earthquakes reveal the critical state of the crust

corresponding to  $n$  close to 1 while large earthquakes move the crust away from criticality so that their triggered aftershock sequences correspond to a small branching ratio  $n < 1$ , hence the larger exponent. This picture has been recently advocated under the concept of "intermittent criticality" (see for instance [Jaume and Sykes, 1999; Goltz and Bose, 2002; Ben-Zion et al., 2003; Bowman and Sammis, 2004]). While we cannot exclude that intermittent criticality is the explanation for our results, this interpretation has only qualitative predictive power and needs more fine-tuning than the multifractal stress activation model since the latter predicts precisely the observed linear dependence of  $p(M)$ . For the ETAS model to explain our results, we would need a magnitude dependence of the productivity parameter which does not seem to be observed [Helmstetter, 2003] (note however that Helmstetter's measure of  $\lambda$  are probably underestimated as they have relied on the assumption of a constant  $p$ -value and have used a fixed space domain size independent of mainshock magnitude to select them). In addition, the multifractal stress activation model is physically-based while the ETAS model is only phenomenological and less attractive as an "explanation."

## 6.5. Other predictions of the multifractal stress activation model

### 6.5.1. Temperature dependence of $p$ -values

Another prediction of the multifractal stress activation model is the linear dependence of the  $p$ -value /  $\lambda$  in (37) as a function of the inverse of the temperature. This implies that the strong dependence of the  $p$ -value as a function of mainshock magnitude should be more visible with a larger amplitude for cold regions. This suggests a tantalizing new interpretation of the correlations reported between the  $p$ -value and thermal flux [Kisslinger and Jones, 1991]. These authors observed a positive correlation, specially in line with the intuitive idea that hotter material relaxes stress at larger rates. We must point out, however, that they did not take account of uncertainties on measured heat flow, and that such a correlation was obtained by inverting  $p$  on a few dozens of individual aftershock sequences following mainshocks of different magnitudes (from 5.1 to 7.5). Using a world-wide catalog of events of magnitudes larger than 5, within which they selected nine subregions, Marsan and Bean

[2003] also observed a positive correlation between  $p$  and heat-flow. The exponent  $p$  was computed through the estimation of the power-spectrum of the time-series of events. Their figure 10 shows error bars on both  $p$  and heat-flow. Despite the rather strong apparent correlation, we would like to stress that such results are difficult to interpret because the data points are concentrated around average heat-flow values, and there are only a few data for very large or very small heat-flow values. Thus, the dispersion of data is highly inhomogeneous around the mean and such a biased sampling in heat-flow may yield misleading results. Here, again we propose to reconsider such an analysis with a more uniform sampling in heat-flow and according to the magnitude of main events. Indeed, since our model predicts that the magnitude and temperature effects are entangled, a careful analysis of the magnitude relationship  $p(M)$  is needed before testing for a temperature or heat-flow effect.

We predict a negative correlation between  $p$  and temperature which seems at first rather puzzling, as it predicts that the seismicity rate will relax more slowly at larger temperatures (every other parameter being kept equal). This paradox is resolved by distinguishing between absolute seismicity rate and relative decay rates. Indeed, expressions (1) and (2) show that the seismic rate can be decomposed into the product of two exponential terms

$$(\dot{\epsilon}; t) = e^{E_0(\epsilon)} e^{+V(\epsilon; t)}; \quad (47)$$

The first exponential  $e^{E_0(\epsilon)}$  controls the absolute seismicity level and exhibits the usual effect that, the higher the temperature  $kT = 1/\beta$ , the larger is the seismicity rate. The second exponential  $e^{+V(\epsilon; t)}$  gives the dependence of the seismicity rate as a function of time due to stress interactions, as described in (3) and following equations. It exhibits an inverse temperature effect: the larger the temperature, the smaller it is; together with the dependence  $(\dot{\epsilon}; t) / \ln(T=t)$ , it is responsible for the paradoxical temperature dependence of the  $p$ -value. In summary, the larger the temperature, the larger is the absolute seismicity level but the smaller is the  $p$ -value of Omori's law. More generally, distinguishing between absolute and relative levels is essential when dealing with scale-invariant laws. The same paradoxical effect occurs for instance with fractal dimensions: a large fractal dimension

does not necessarily imply a large density, since the density is the product of an absolute term setting the units and a scale-dependent part function of the fractal dimension: the fractal dimension only describes the relative values of densities at two different scales, not their absolute values. Confusing these two contributions to the density is often done in the geophysical literature in which the dimension is incorrectly considered as a first-order measure of density; in reality, it is only a relative measure comparing densities at different scales. To come back to Kisslinger and Jones [1991]'s observations, rather than large  $p$ -values associated with large heat flows, we suggest a more complicated dependence involving a higher absolute seismicity level and a weaker dependence of  $p$  on the mainshock magnitude as the temperature (heat flow) increases. Everything being kept equal, as the temperature increases, the  $p(M)$  values are predicted to decrease. This may perhaps also explain the careful laboratory observations of Carreker [1950] who showed for Pt (platinum) that the strain rate exponent in creep experiments in the primary regime decreases with temperature. Some other complications can occur if the integral time scale  $T$  also depends on the temperature, but if it is very large as we expect (at least a few years), its variation with the temperature  $1/T$  will not have significant consequences for the seismic aftershock decay rates studied here.

The decrease of  $p$  with increasing temperature has been also documented in a numerical simulation of the sandpile model of Christensen and Olami [1992] in which elements break by static fatigue according to the rate (1) with (2). It was found [Helmstetter, 2002] that this decrease of  $p$  with  $T$  is the opposite of the prediction of the standard thermal activation model when neglecting interactions between rupture and thus results fundamentally from multiple interactions between events.

#### 6.5.2. Magnitude-dependence of the $p$ -values in other works

The increase of the  $p$ -value with the mainshock magnitude implies that aftershock sequences of large events decay at a faster rate than aftershock sequences of small events. Yet, they have a much larger number of events and can thus be observed in general over longer times. According to our analysis, mainshocks of magnitudes going from 5 and 7.5 (for which the Omori law is generally



inverted), the average  $p$ -value increases from 0.9 to 1.2. These are the typical values generally given in the literature. Our detection of a systematic increase of  $p(M_L)$  was only made clear by extending the range of magnitudes over which the Omori law is tested.

There has been only few attempts to try to correlate  $p$ -values of individual aftershock time-series with the magnitude of the mainshock (see Kisslinger and Jones, 1991], for example, in which no correlation was found which is not surprising as our analysis shows that one has to stack many sequences following similar magnitude shocks in order to average fluctuations out). The only other work we are aware, which uses stacked sequences, is the one of Bohnenstiehl et al. [2003]. These authors studied the time-clustering of events of magnitude  $M > 3$  along the Mid-Atlantic Ridge, using catalogs derived from the detection of T-waves. Each event is quantified using a source level (SL), expressed in dB units, which is a logarithmic measure of its size. The earthquake catalog is then represented as a series of point process events located at each earthquake's occurrence time, whose power spectrum can be computed and fitted with a power law of exponent  $p_s$  (they indeed use an Allan factor analysis to determine  $p_s$ ). Tuning the detection threshold  $SL_0$  of events, they note a tendency for  $p_s$  to decrease as  $SL_0$  increases. Since the  $p$ -value is related to  $p_s$  by  $p = 1 - p_s$ , then their observation confirms that  $p$  decreases with  $M$  (since, due to the Gutenberg-Richter law, their power-spectrum is dominated by the statistics related to the smallest magnitude events in the catalogue).

Mines or meso-scale crustal laboratories to study superficial earthquakes. The sizes of events are most often of magnitude 3 and lower. As stated above, such events trigger a few aftershocks so that the recovery of an Omori law requires stacking many events. Marsan et al. [1999] studied the time clustering of events in the Creighton mine (Ontario, Canada), and built a stacked time-series which is equivalent to ours if we consider that the size of the aftershock area after each event is the size of the mine itself. Despite the fact that they did not remove shocks already tagged as aftershocks from the main events list (which is a minor departure from our procedure considering the small size of all events), they measured  $p = 0.4$ . They do not mention the magnitude range of events they used in their paper, but such a  $p$ -value suggests (from our observations) that the majority of their shocks would roughly be

of magnitude 1.3, which is a very reasonable prediction for such events. According to our model, we should also take into account the difference of temperature to get a reliable quantitative comparison, but the low p-value found by Marsan et al. [1999] is already in qualitative agreement with our model.

### 6.5.3. Dependence of the p-value on the shear and normal stress components

The multifractal stress activation model may rationalize the empirical observations of a dependence of the p-value on the shear and normal stress components, which suggests the relevance of fluid pressure [Scholz, 2002]. These properties which cannot be accounted for by the Dieterich model [Dieterich, 1994] can naturally arise from the impact of fluid pressure on the stress redistribution.

### 6.5.4. Distribution of seismic rates and of stress source strengths

Our multifractal stress activation model can be further falsified by comparing its prediction of the distribution of seismic rates  $P_r(\cdot)$ , once the distribution (12) of stress source strengths and the stress relaxation memory kernel (13) are specified. As  $P_r(\cdot)$  seems to be a power law with exponent 1.5 [Work in progress], this seems to imply a truncation of the distribution of the stress source strengths. More work is required to clarify this issue and will be reported elsewhere.

### 6.5.5. Implications for prediction

If true, our discovered multifractal Omori law has probably many important implications for understanding earthquake patterns and for prediction, that need to be investigated in details. The interplay between magnitude and decay rate found here leads to new interpretations of spatio-temporal patterns of seismicity. In particular, this will shed light on the underlying basis of various pattern recognition techniques that tend to sort earthquakes in terms of their magnitudes: according to our theory, different magnitude classes which are controlled by the same underlying physics give rise to distinct triggering signatures.

### 6.5.6. Lower bounds for a minimum earthquake magnitude

The reported dependences (42) and (43) of  $p(M_L)$  suggests the existence of a lower bound  $M_{min}$  for the minimum magnitude of earthquake able to trigger other events. Indeed, from the condition  $p = 0$ , we obtain  $M_{min} > 2.3$  using (42) and  $M_{min} > 3.7$  (43). The real uncertainty is difficult to estimate and is probably of the order of the difference between these two values. Since there is no way we can address all known and unknown systematic error terms and uncertainties, the best way to estimate the uncertainty is by comparison of two different procedures with several different implementation, as we have done. This leads to the estimate  $M_{min} > 3 \pm 1$ . Note that the existence of  $M_{min}$  does not imply that there are no earthquakes of smaller magnitudes, only that those smaller events do not play a role in the triggering process (they do not trigger other events).

Acknowledgments. We are grateful to K. Felzer, Y. Y. Kagan, J.-F. Muzy and J. Vidale for stimulating discussions. This work was partially supported by NSF-EAR 02-30429 and by the Southern California Earthquake Center (SCEC).

## R e f e r e n c e s

- Atkinson, B. K. et al., Mechanisms of fracture and friction of crustal rock in simulated geologic environments, supported by the Earthquake Hazards Reduction Program, [Menlo Park, Calif.] : U.S. Geological Survey, 81-277, 1981.
- Atkinson, B. K., Subcritical crack growth in geological materials, *J. Geophys. Res.*, 89, 4077-4114, 1984.
- Baumberger, T., Contact dynamics and friction at a solid-solid interface: material versus statistical aspects, *Solid State Commun.*, 102, 175-185, 1997.
- Baumberger, T., P. Berthoud, C. Caroli, Physical analysis of the state- and rate-dependent friction law, II. Dynamic friction, *Phys. Rev. B*, 60, 3928-3939, 1999.
- Bebbington, M. and Harte, D., The linked stress release model for spatio-temporal seismicity: formulations, procedures and applications, *Geophys. J. Int.*, 154, 925-946, 2003.
- Ben-Zion, Y., Eneva, M. and Liu, Y. F., Large earthquake cycles and intermittent criticality on heterogeneous faults due to evolving stress and seismicity, *J. Geophys. Res.*, 108 (B6), 2307, 2003.
- Bohnenstiehl, D. R., Tolstoy, M., Smith, D. K., Fox, C. G. and Dziak, R. P., Time-clustering behavior of spreading-center seismicity between 15 and 35°N on the Mid-Atlantic Ridge: observations from hydroacoustic monitoring, *Phys. Earth Planet. Inter.*, 138, 147-161, 2003.
- Borovkov, K. and Bebbington, M. S., A simple two-node stress transfer model reproducing Omori's law, *Pure Appl. Geophys.*, 160, 1429-1445, 2003.
- Bowman, D. D. and Sammis, S. G., Intermittent Criticality and the Gutenberg-Richter Distribution, in press in *Pure & Applied Geophys.*, 2004.

- Brechet, Y., Y. Estrin, The effect of strain rate sensitivity on dynamic friction of metals, *Scripta Metall.*, 30, 1449-1445, 1994.
- Bremaud, P. and Massoulié, L., Stability of nonlinear Hawkes processes, *The Annals of Probability*, 24, 1563-1588, 1996.
- Bremaud, P., Nappo, G. and Torrisi, G.L., Rate of convergence to equilibrium of marked Hawkes processes, *J. Appl. Prob.*, 39, 123-136, 2002.
- Calais, E., Vergnolle, M., Deverchère, J., San'kov, V., Lukhnev, A. and Amara-jargal S., Are post-seismic effects of the  $M = 8.4$  Bolnay earthquake (1905 July 23) still influencing GPS velocities in the Mongolia-Baikal area? *Geophys. J. Int.*, 149, 157-168, 2002.
- Carreker, R.P. Jr., *J. Appl. Phys.*, 21, 1289-1296, 1950.
- Chester, F.M., Effects of temperature on friction: Constitutive equations and experiments with fault gouge, *J. Geophys. Res.*, 99, 7247-7261, 1994.
- Chester, F.M. and Higgs, N., Multimechanism friction constitutive model for ultra fine quartz gouge at hypocentral conditions, *J. Geophys. Res.*, 97, 1859-1870, 1992.
- Christensen, K. and Zölami, Variation of the Gutenberg-Richter b-values and non-trivial temporal correlation in a spring-block model for earthquakes, *J. Geophys. Res.*, 97, 8729-8735, 1992.
- Chung, S.H., and J.R., Stevens, Time-dependent correlation and the evaluation of the stretched exponential or Kohlrausch-Williams-Watts function, *Am. J. Phys.*, 59, 1024-1030, 1991.
- Ciliberto, S., A. Guarino and R. Scorretti, The effect of disorder on the fracture nucleation process, *Physica D*, 158, 83-104, 2001.
- Deng, J., M. Gurnis, H. Kanamori and E. Hauksson, Viscoelastic flow in the lower crust after the 1992 Landers, California, earthquake, *Science*, 282, 1689-1692, 1998.

- Dieterich, J., Modelling of rock friction: 1. Experimental results and constitutive equations. *J. Geophys. Res.*, 84, 2161-2168, 1979.
- Dieterich, J., A constitutive law for rate of earthquake production and its application to earthquake clustering, *J. Geophys. Res.*, 99 (B2), 2601-2618, 1994.
- Felzer, K. R., Abercrombie, R. E. and Ekstrom, G., A common origin for aftershocks, foreshocks, and multiplets, *Bull. Seism. Soc. Am.*, 94 (1), 88-98, 2004.
- Freed, A. M. and J. Lin, Delayed triggering of the 1999 Hector Mine, California quake by the 1992 Landers quake due to lower crustal flow: implications for loading of the southern San Andreas Fault, *EOS Trans. AGU Fall 2000 Meeting Abstracts* (48, suppl.), 81, p. F860, 2000.
- Freed, A. M. and Lin, J., Delayed triggering of the 1999 Hector Mine earthquake by viscoelastic stress transfer, *Nature*, 411, 180-183, 2001.
- Goltz, C. and Bose, M., Configurational entropy of critical earthquake populations, *Geophys. Res. Lett.*, 29 (20), 1990, 2002.
- Griggs, D. T., F. J. Turner and H. C. Heard, Deformation of rocks at 500 °C and 800 °C, *Geol. Soc. Am. Memoir*, 79, 39-104, 1957.
- Griggs, D. T., and J. Handin, editors, Rock deformation (A symposium), *Geol. Soc. Am. Memoir*, 79, 381 pages, 1960.
- Halsey, T. C., Jensen, M. H., Kadanoff, L. P., Procaccia, I., Shraiman, B. I., Fractal measures and their singularities: the characterization of strange sets, *Phys. Rev. A* 33, 1141-1151, 1986.
- Hawkes, A. G., Point spectra of some mutually exciting point processes. *Journal of Royal Statistical Society, series B*, 33, 438-443, 1971.

- Helmstetter, A., Ruptures et Instabilités: sismicité et mouvements gravitaires, PhD thesis, Univ. Grenoble, unpublished, 2002.
- Helmstetter, A., Is Earthquake Triggering Driven by Small Earthquakes? *Phys. Rev. Lett.*, 91, 058501, 2003.
- Helmstetter, A. and D. Sornette, Sub-critical and supercritical regimes in epidemic models of earthquake aftershocks, *J. Geophys. Res.*, 107, 2237, doi:10.1029/2001JB001580, 2002a.
- Helmstetter, A. and D. Sornette, Diffusion of epicenters of earthquake aftershocks, Omori's law, and generalized continuous-time random walk models, *Phys. Rev. E*, 6606, 061104, 2002b.
- Helmstetter, A. and D. Sornette, Foreshocks explained by cascades of triggered seismicity, *J. Geophys. Res.*, 108 (B10), 2457, doi:10.1029/2003JB002409, 2003a.
- Helmstetter, A. and D. Sornette, Bath's law Derived from the Gutenberg-Richter law and from Aftershock Properties, *Geophys. Res. Lett.*, 30, 2069, doi:10.1029/2003GL018186, 2003.
- Heslot, F., T. Baumbarger, B. Perrin, B. Caroli, and C. Caroli, Creep, stick-slip, and dry friction dynamics: experiments and a heuristic model, *Phys. Rev. E*, 49, 4973-4988, 1994.
- Huang, Y., A. Johansen, M. W. Lee, H. Saleur and D. Sornette, Artifactual Log-Periodicity in Finite-Size Data: Relevance for Earthquake Aftershocks, *J. Geophys. Res.*, 105, 25451-25471, 2000.
- Huc, M. and Main, I.G., Anomalous stress diffusion in earthquake triggering: Correlation length, time dependence, and directionality, *J. Geophys. Res.*, 108 (B7), 2324, 2003.
- Imoto, M., Mameda, K. and Yoshida, A., Use of statistical models to analyze periodic seismicity

- observed for clusters in the Kanto region, central Japan, *Pure Appl. Geophys.*, 155, 609-624, 1999.
- Jackson, D.D., Shen, Z.K., Potter, D., Ge, X.B. and Sung, L.Y., Southern California deformation, *Science*, 277, 1621-1622, 1997.
- Jaume, S.C. and Sykes, L.R., Evolving towards a critical point: A review of accelerating seismic moment/energy release prior to large and great earthquakes, *Pure & Applied Geophys.*, 155 (2-4), 279-305, 1999.
- Kagan, Y.Y., Distribution of incremental static stress caused by earthquakes, *Nonlinear Processes in Geophysics*, 1, 171-181, 1994.
- Kagan, Y.Y., Accuracy of modern global earthquake catalogs, *Phys. Earth & Plan. Int.*, 135 (2-3), 173-209, 2003.
- Kagan, Y.Y., Short-term properties of earthquake catalogs and models of earthquake source, *Bull. Seism. Soc. Am.*, in press, 2004.
- Kagan, Y.Y. and D.D. Jackson, Spatial aftershock distribution: Effect of normal stress, *J. Geophys. Res.*, 103, 24453-24467, 1998.
- Kagan, Y.Y. and L. Knopov, Stochastic synthesis of earthquake catalogs, *J. Geophys. Res.*, 86, 2853-2862, 1981.
- Kagan, Y.Y. and L. Knopov, Statistical short-term earthquake prediction, *Science*, 236, 1563-1467, 1987.
- Kenner, S.J., and P. Segall, Time Dependence of the Stress Shadowing Effect and Its Relation to the Structure of the Lower Crust, *Geology*, 27, 119-122, 1999.
- King, G.C.P., Stein, R.S. and Lin, J., Static stress changers and the triggering of earthquakes, *Bull. Seism. Soc. Am.*, 84 (3), 935-953, 1994.



- Kisslinger, C. and Jones, L.M., Properties of aftershock sequences in southern California, *J. Geophys. Res.*, 96 (B7), 11947-11958, 1991.
- Klinger, M.I., Glassy disordered systems: topology, atomic dynamics and localized electron states, *Phys. Rep.*, 165, 275-397, 1988.
- Lapusta, N., J.R. Rice, Y. Ben-Zion and G. Zheng, Elastodynamic analysis for slow tectonic loading with spontaneous rupture episodes on faults with rate- and state-dependent friction, *J. Geophys. Res.*, 105, 23,765-23,789, 2000.
- Lee, M.W. and D. Sornette, Novel mechanism for discrete scale invariance in sandpile models, *European Physical Journal B*, 15, 193-197, 2000.
- Lin, J. and Stein, R.S., Stress triggering in thrust and subduction earthquakes and stress interaction between the southern San Andreas and nearby thrust and strike-slip faults, *J. Geophys. Res.* 109 (B2), 2303, 2004.
- Liu, J.Y., Ross, R.J., Energy criterion for fatigue strength of wood structural members, *Journal of Engineering Materials and Technology* 118 (3), 375-378, 1996.
- Liu, J., Vere-Jones, D., Ma, L., Shi, Y. and Zhuang, J.C., The principle of coupled stress release model and its application, *Acta Seismologica Sinica*, 11, 273-281, 1998.
- Marsan, D., Triggering of seismicity at short timescales following Californian earthquakes, *J. Geophys. Res.*, 108 (B5), 2266, 2003.
- Marsan, D. and Bean, C., Seismicity response to stress perturbations, analysed for a world-wide catalogue, *Geophys. J. Int.*, 154, 179-195, 2003.
- Murnu, M., Console, R. and Lisi, A., Seismicity and mean magnitude variations correlated to the strongest earthquakes of the 1997 Umbria-Marche sequence (central Italy), *J. Geophys. Res.*, 109 (B1), 1304, 2004.

- Muzy, J.-F. and E. Bacri, Multifractal stationary random measures and multifractal random walks with logarithmically divisible scaling laws, *Phys. Rev. E*, 66, 056121, 2002.
- Nakatani M., Conceptual and physical clarification of rate and state-dependent friction law: Thermally activated rheology of frictional sliding, *J. Geophys. Res.*, 106, 13347-13380, 2001.
- Ogata, Y., Statistical models for earthquake occurrence and residual analysis for point processes, *J. Am. stat. Assoc.*, 83, 9-27, 1988.
- Papazachos, B.C., Karakaisis, G.F., Papazachos, C.B. and Scordilis, E.M., Earthquake triggering in the north and east Aegean plate boundaries due to the Anatolia westward motion, *Geophys. Res. Lett.*, 27 (23), 3957-3960, 2000.
- Parisi, G. and Frisch, U., On the singularity structure of fully developed turbulence, in *Turbulence and Predictability in Geophysical Fluid Dynamics*, Proceedings International School Enrico Fermi, 1983, Varenna, Italy, eds. Ghil, M., Benzi, R. and Parisi, G. (North Holland, Amsterdam, 1985).
- Perfettini, H. and J.-P. Avouac, Postseismic relaxation driven by brittle creep: A possible mechanism to reconcile geodetic measurements and the decay rate of aftershocks, application to the Chi-Chi earthquake, Taiwan, *J. Geophys. Res.*, 109, B02304, doi:10.1029/2003JB002488, 2004.
- Perfettini, H., Schmittbuhl, J. and Cochard, A., Shear and normal load perturbations on a two-dimensional continuous fault: 2. Dynamic triggering, *J. Geophys. Res.*, 108 (B9), 2409, 2003.
- Persson, B.-N.J., *Sliding Friction: Physical principles and applications* (Springer, Heidelberg, 2000).

- Phillips, J.C., Stretched exponential relaxation in molecular and electronic glasses, *Rep. Prog. Phys.*, 59, 1133-1208, 1996.
- Politi, A., S. Ciliberto and R. Scorretti, Failure time in the fiber-bundle model with thermal noise and disorder, *Phys. Rev. E*, 66, 026107, 2002.
- Pollitz, F.F., Peltzer, G. and Buergmann, R., Mobility of continental mantle; evidence from postseismic geodetic observations following the 1992 Landers earthquake, *J. Geophys. Res. B*, 105, 8035-8054, 2000.
- Ruina, A.L., Slip instability and state variable friction laws, *J. Geophys. Res.*, 88, 10359-10370, 1983.
- Saichev, A. and D. Sornette, Andrade, Omori and Time-to-failure Laws from Thermal Noise in Material Rupture, submitted to *Phys. Rev. Lett.* (<http://arXiv.org/abs/cond-mat/0311493>), 2003.
- Schmitt, F.G., A causal multifractal stochastic equation and its statistical properties, *Eur. Phys. J. B*, 34 (1), 85-98, 2003.
- Schmitt, F. and Marsan, D., Stochastic equations generating continuous multiplicative cascades, *Eur. Phys. J. B*, 20 (1), 3-6, 2001.
- Scholz, C.H., Earthquakes and friction laws, *Nature*, 391, 37-42, 1998.
- Scholz, C.H., The mechanics of earthquakes and faulting (Cambridge, UK; New York: Cambridge University Press, 2nd ed., 2002).
- Scholz, C.H. and Engelder, T., Role of asperity indentation and ploughing in rock friction, *Int. J. Rock Mech. Min. Sci.*, 13, 149-154, 1976.
- Shi, Y., Liu, Y., Vere-Jones, D., Zhuang, J. and Ma, I., Application of mechanical and statistical models to the study of seismicity of synthetic earthquakes and the prediction

- of natural ones, *Acta Seismologica Sinica*, 11, 421-430, 1998.
- Sleep, N. H., Application of a unified rate and state friction theory to the mechanics of fault zones with strain localization, *J. Geophys. Res.*, 102, 2875-2895, 1997.
- Somette, A. and D. Somette, Renormalization of earthquake aftershocks, *Geophys. Res. Lett.*, 6, 1981-1984, 1999.
- Somette, D., Earthquakes: from chemical alteration to mechanical rupture, *Physics Reports*, 313 (5), 238-292, 1999.
- Somette, D., *Critical Phenomena in Natural Sciences, Chaos, Fractals, Selforganization and Disorder: Concepts and Tools*, 2nd ed. (Springer Series in Synergetics, Heidelberg, 2004).
- Somette, D. and K. Ide, The Kalman-Levy filter, *Physica D*, 151, 142-174, 2001.
- Somette, D., Y. Malevergne and J.-F. Muzy, What causes crashes? *Risk*, 16 (2), 67-71, 2003.
- Stein, R. S., Earthquake conversations, *Scientific American*, 288 (1), 72-79, 2003.
- Stesky, R. M., Mechanisms of high temperature frictional sliding in wetly granite, *Can. J. Earth Sci.*, 15, 361-375, 1977.
- Vere-Jones, D., Earthquake prediction: a statistician's view, *J. Phys. Earth*, 26, 129-146, 1978.
- Voisin, C., Dynamic triggering of earthquakes: The nonlinear slip-dependent friction case, *J. Geophys. Res.*, 107 (B12), 2356, 2002.
- Vulliamy, L., Natural slopes in slow movement, in *Modeling in geomchanics*, edited by M. Zamani, G. Giorda, and J. Booker (John Wiley, Chichester, U.K., 2000) pp. 654-676.
- Wang, W. and Scholz, C. H., Micromechanics of the velocity and normal stress dependence of rock friction, *Pure Appl. Geophys.*, 143, 303-316, 1994.
- Wells, D. L. and Coppersmith, K. J., New empirical relationships among magnitude, rupture

length, rupture width, rupture area, and surface displacement, *Bull. Seism. Soc.*

*Am.*, 84 (4), 974-1002, 1994.

Zheng, X. and Vere-Jones, D., Applications of stress release models to earthquakes from North China, *Pure and Applied Geophysics*, 135, 559-576, 1991.

Zhurkov, S.N., Kinetic concept of the strength of solids, *Int. J. Fract. Mech.*, 1, 311-323, 1965.

Zolotarev, V.M., One-dimensional Stable Distributions, *Amer. Math. Soc. Providence R.I.*, 1986.

Zolotarev, V.M. and Strunin, B.M., Internal-stress distribution for a random distribution of point defects, *Soviet Phys. Solid State*, 13, 481-482, 1971.

---

Guy Ouillon, Department of Earth and Space Sciences and Institute of Geophysics and Planetary Physics, University of California, Los Angeles, California and Laboratoire de Physique de la Matière Condensée, CNRS UMR 6622 and Université de Nice-Sophia Antipolis, Parc Valrose, 06108 Nice, France (e-mail: ouillon@aol.com)

Didier Somette, Department of Earth and Space Sciences and Institute of Geophysics and Planetary Physics, University of California, Los Angeles, California and Laboratoire de Physique de la Matière Condensée, CNRS UMR 6622 and Université de Nice-Sophia Antipolis, Parc Valrose, 06108 Nice, France (e-mail: somette@matho.ess.ucla.edu)

Received \_\_\_\_\_

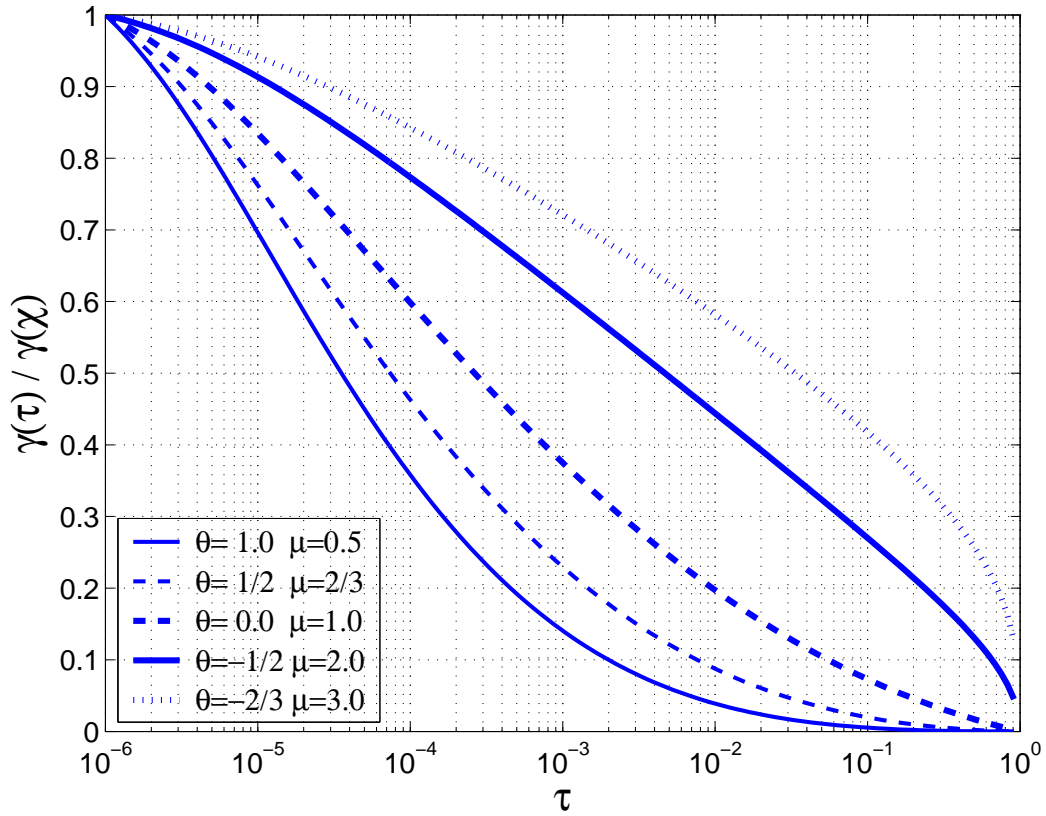


Figure 1. Numerical evaluation of the normalized  $\gamma(\tau) = \gamma(\chi = c=T)$  (linear scale) defined by (31) as a function of  $\tau = t=T$  (logarithmic scale), for several pairs  $(\theta; \mu)$  which obey the condition  $(1 + \mu) = 1$  exactly, using  $c=T = 10^{-6}$ . We verify the existence of a linear decay of  $\gamma(t)$  in the variable  $\ln t$ , which qualifies an Omori power law (36). Since the logarithm of the seismicity rate  $\gamma(t)$  is proportional to  $\ln t$  (with a coefficient of proportionality involving the inverse temperature and the magnitude of the mainshock), a linear behavior qualifies a power law decay of the seismic rate, whose range is rather sensitive to the temperature and the ratio  $c=T$ .

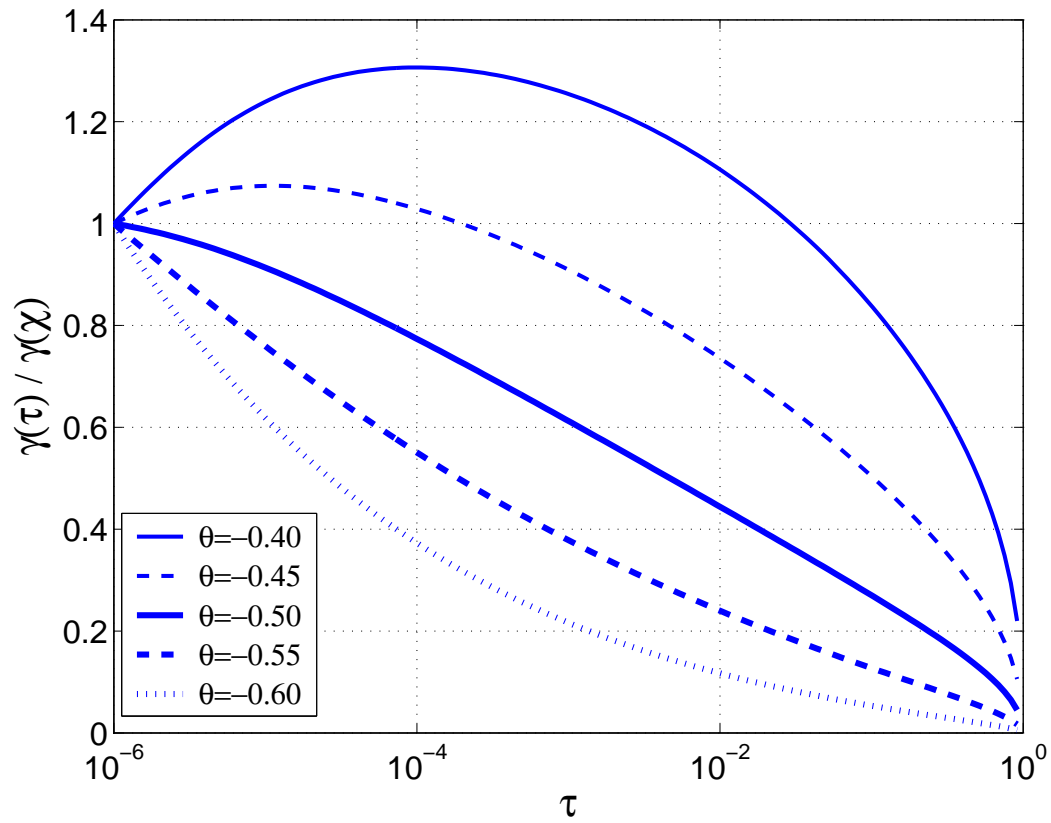


Figure 2. Same as Fig. 1 for several values of  $\theta$  at fixed  $\chi = 2$ , to show the sensitivity of the existence of a linear behavior of  $\chi(t)$  as a function of  $\ln t$  for values of  $(\theta; \chi)$  which depart from the condition  $(1 + \chi) = 1$ . Depending on the temperature and mainshock magnitude, a power law regime for the seismic rate can be observed approximately over several decades even for values of  $(\theta; \chi)$  which depart from the condition  $(1 + \chi) = 1$ .

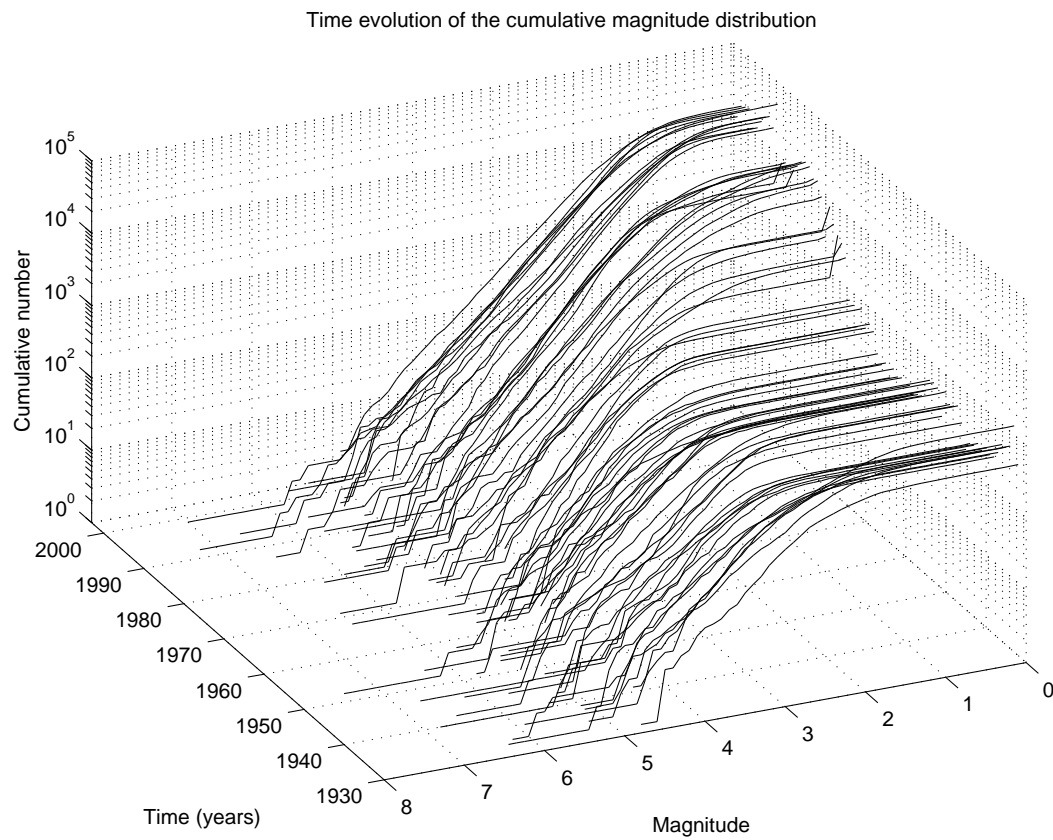


Figure 3. Time evolution of the yearly cumulative magnitude distribution from 1932 to 2003 included, obtained from the Southern Californian earthquakes catalogue with revised magnitudes (available at the Southern California Earthquake Center). Magnitudes  $M_L$  are given with a 0.1 resolution from 1932 to present, in a zone roughly comprised within 32 to 37 N in latitude, and within 114 to 122 in longitude.



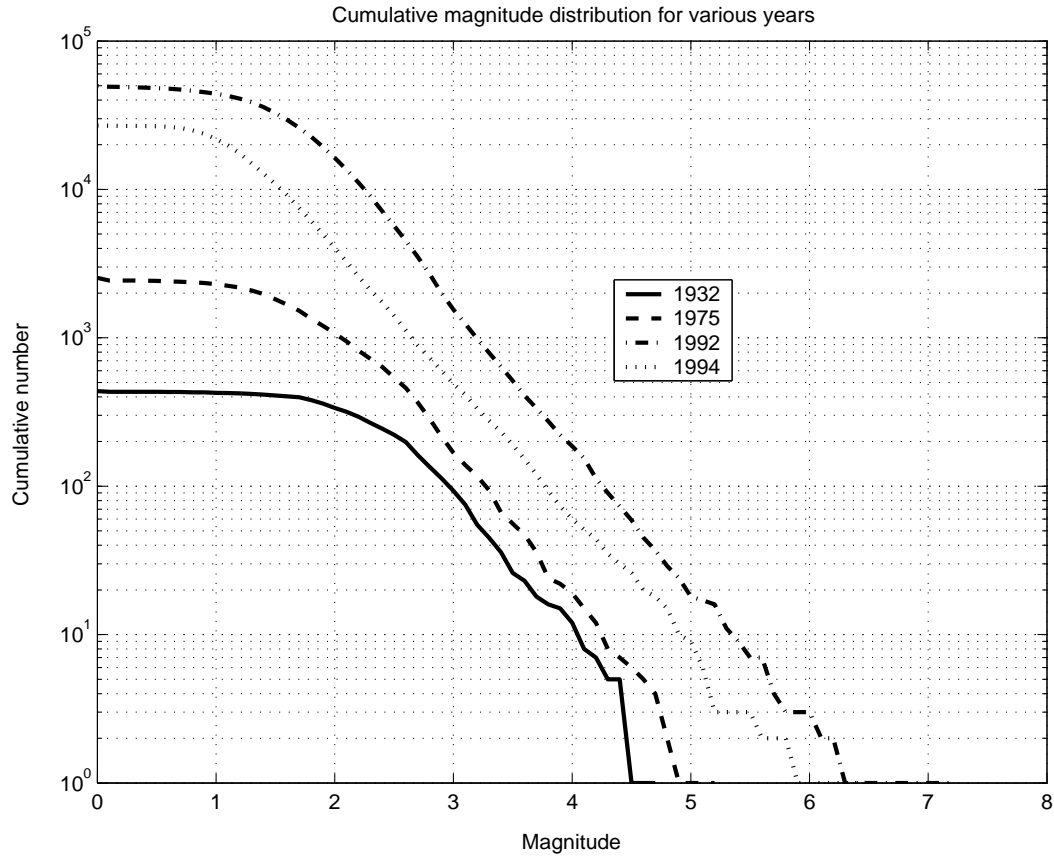


Figure 4. Cumulative magnitude distribution (CMD) for different time spans of the SCEC catalogue used to define the approximate lowest magnitude  $M_L$  of completeness. The CMD is approximately linear for  $M_L > 3$  for the whole lifespan of the catalog, while it is linear for all magnitudes larger than 2.5 (respectively 2 and 1.5) for shocks after 1975 (respectively after 1992 and 1994).

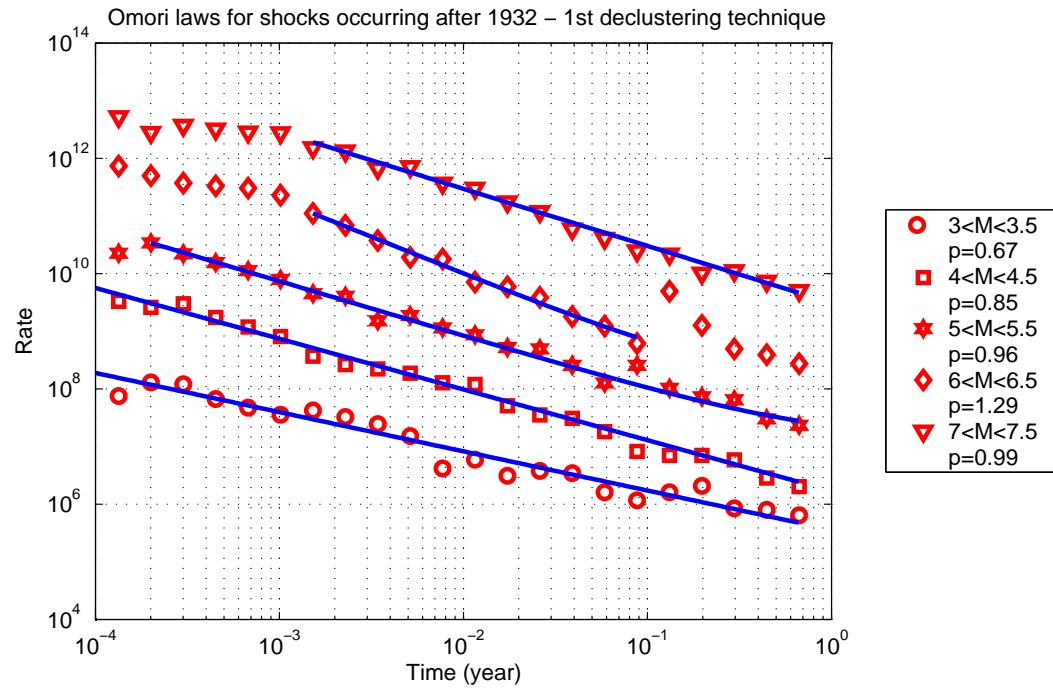


Figure 5. Seismic decay rates of stacked sequences for several magnitude intervals of the mainshocks, for the period from 1932 to 2003 when using the 1st declustering technique.

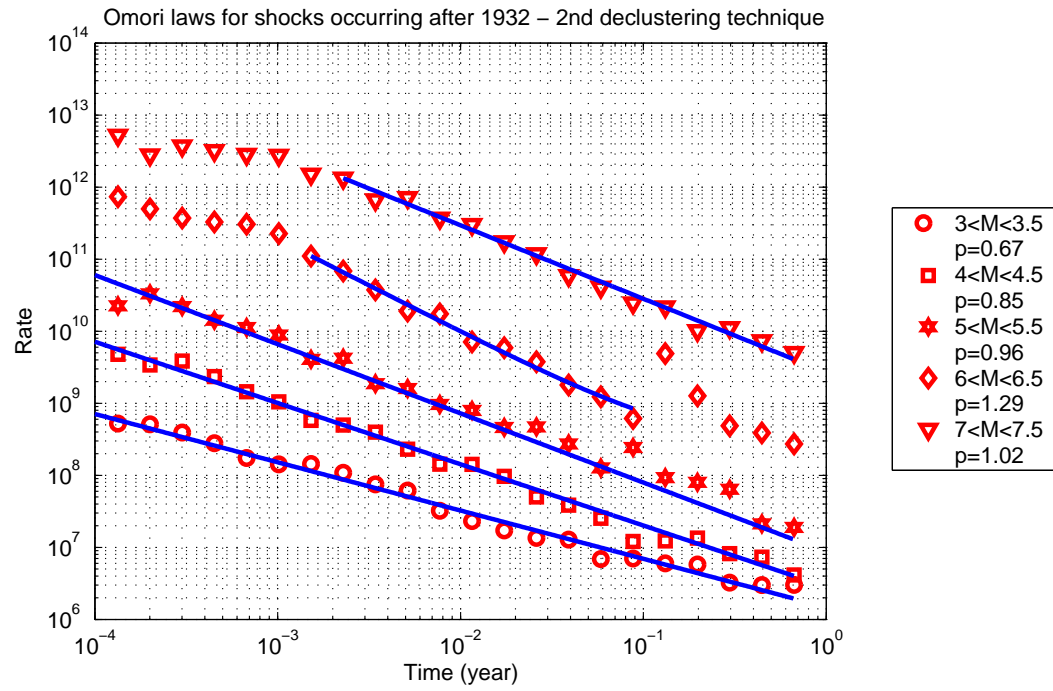


Figure 6. Seismic decay rates of stacked sequences for several magnitude intervals of the mainshocks, for the period from 1932 to 2003 when using the second declustering technique.

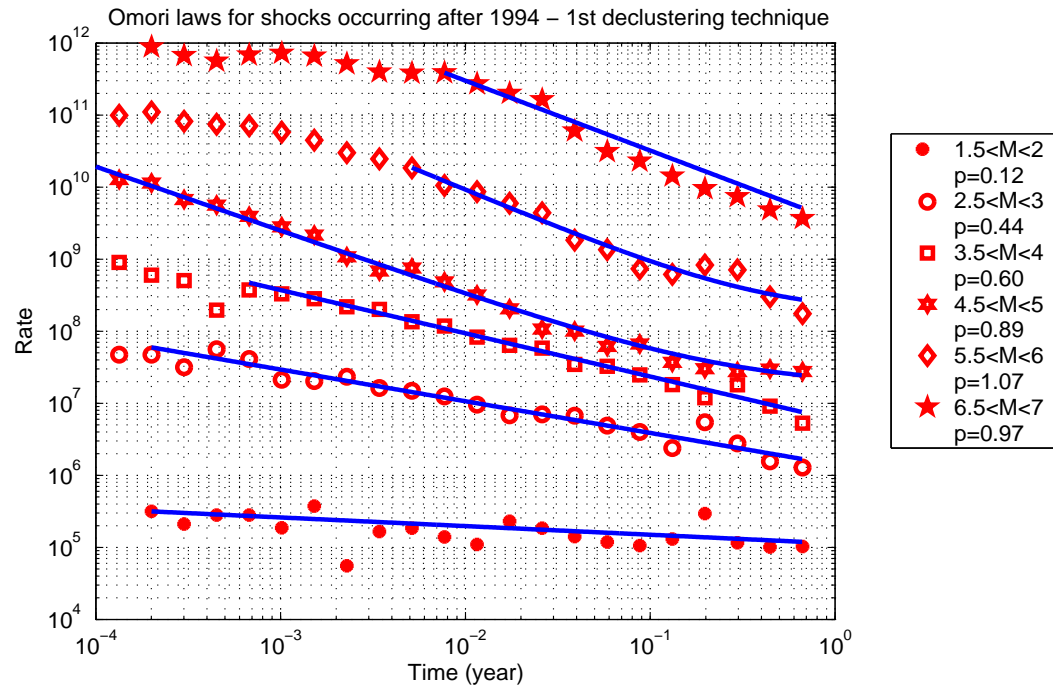


Figure 7. Seismic decay rates of stacked sequences for several magnitude intervals of the mainshocks, for the period from 1994 to 2003 when using the 1st declustering technique.

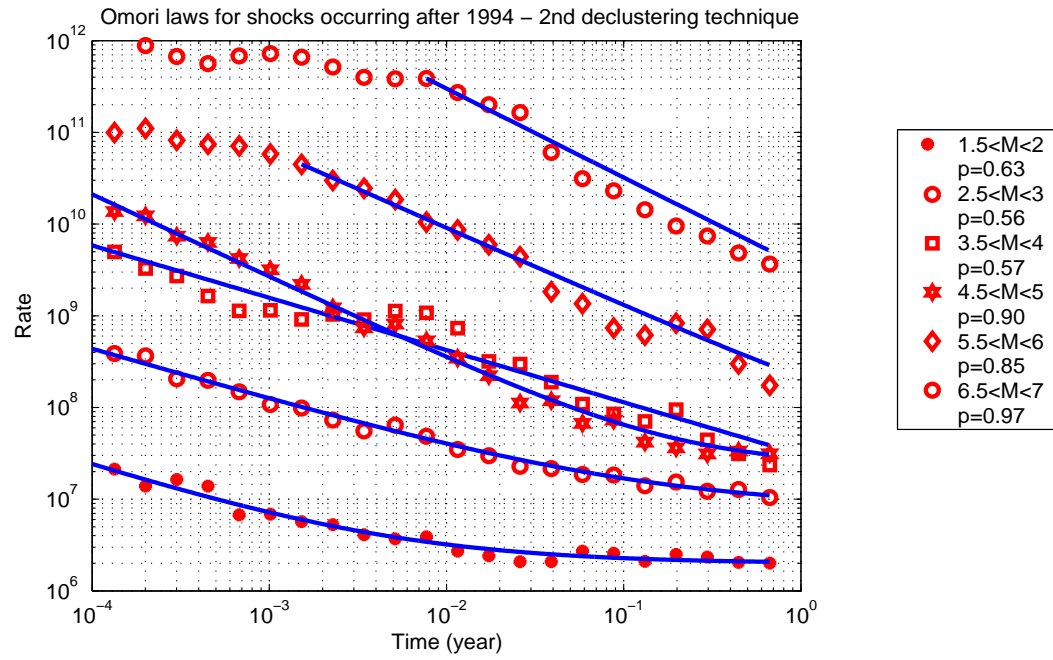


Figure 8. Seismic decay rates of stacked sequences for several magnitude intervals of the mainshocks, for the period from 1994 to 2003 when using the second declustering technique.

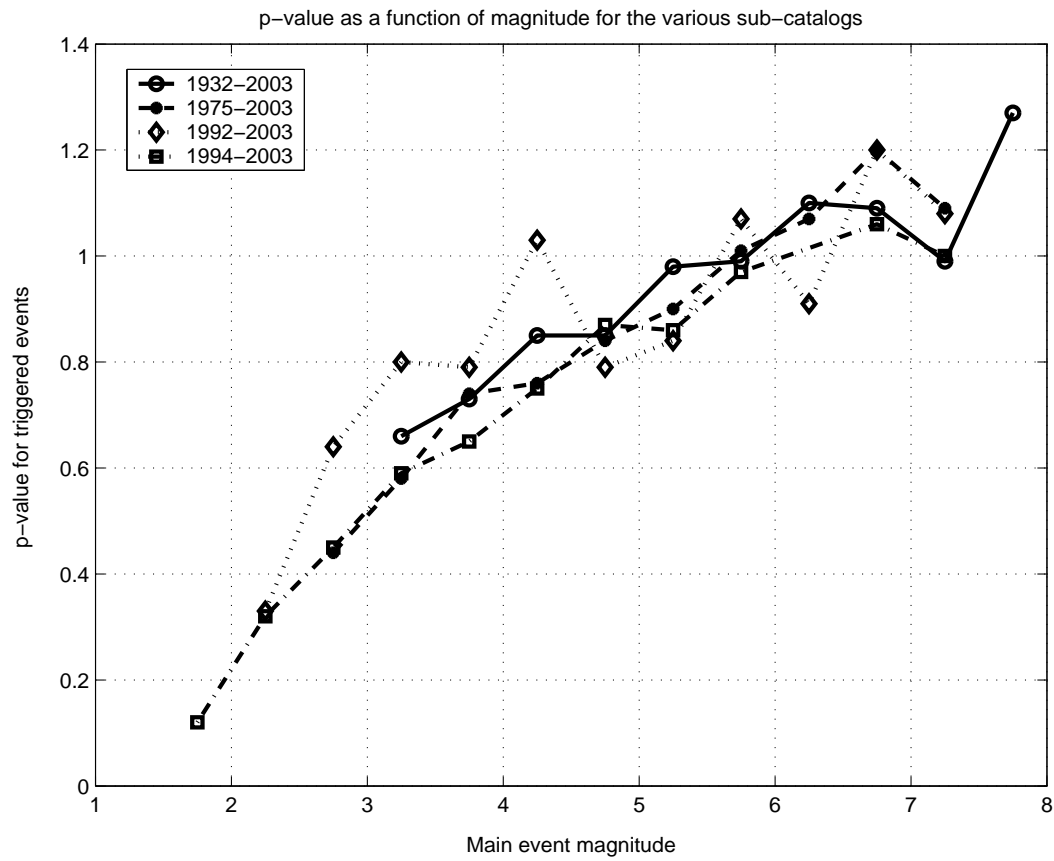


Figure 9. p-values of the Omori law (40) obtained by the procedure described in the text for main shocks (defined using the first declustering algorithm) as a function of the main events' magnitude, for the different sub-catalogs of lifespans given in the inset.

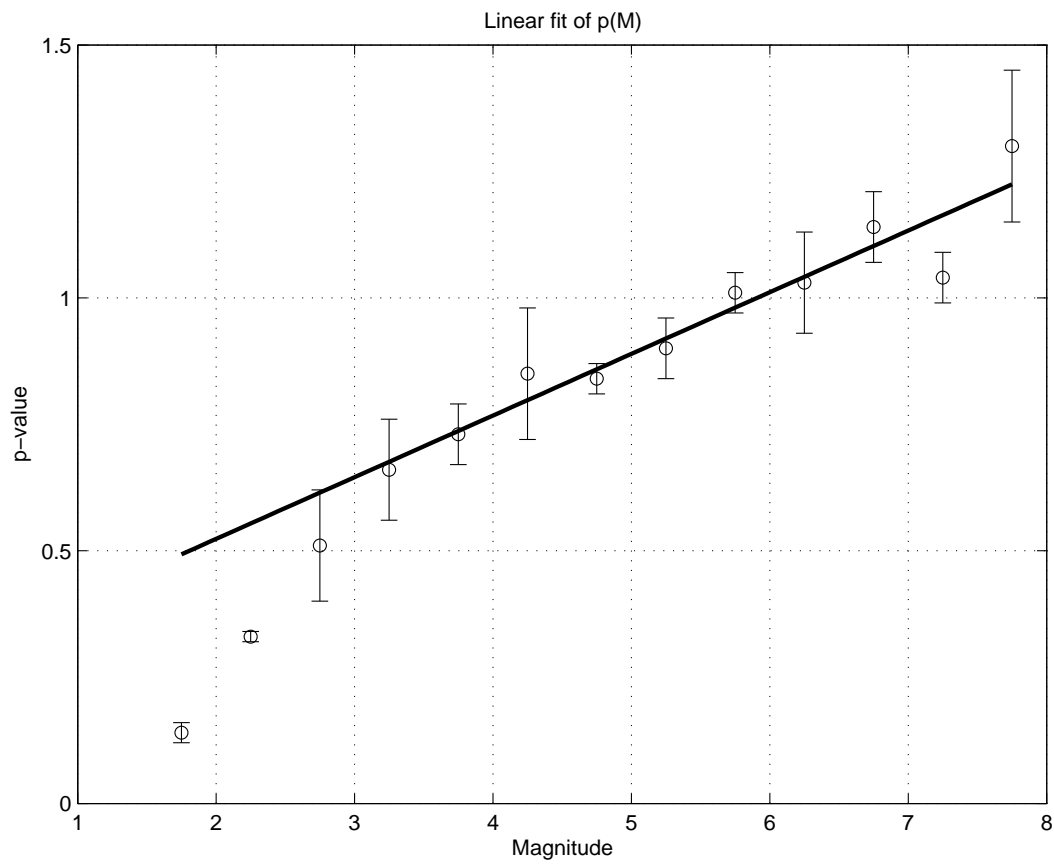


Figure 10. Average p-values and error bars obtained from Figure 9 as described in the text. The straight line is the linear fit with  $p(M) = 0.12M_L + 0.28$ .

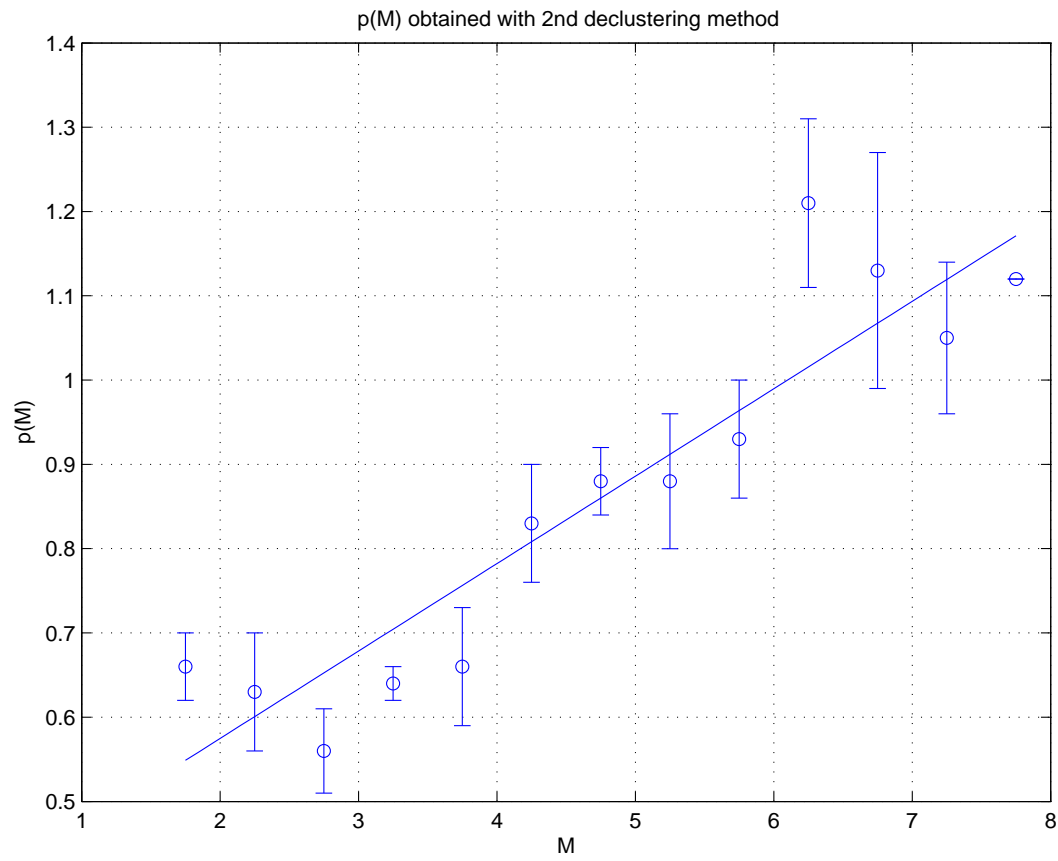


Figure 11. Average p-values and error bars obtained as described in the text using the second declustering technique. The straight line is the linear fit with  $p(M) = 0.10M + 0.37$ .



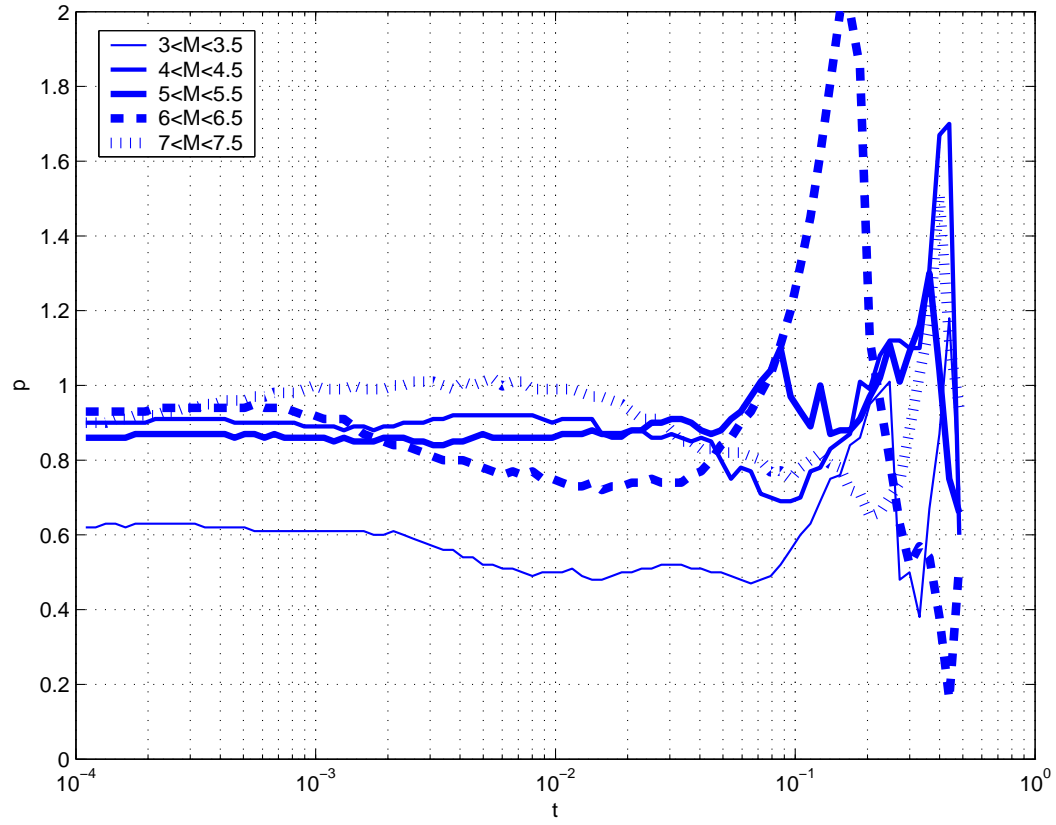


Figure 12. Maximum Likelihood Estimation of the p-value (formula (44) with  $t_0 = 1$  year, while  $t$  was varied continuously from  $10^{-4}$  to 0.5 year) as a function of  $t$  for the post-1932 sub-catalog, using the first declustering technique, with  $R = 2L$ , for different magnitude ranges.

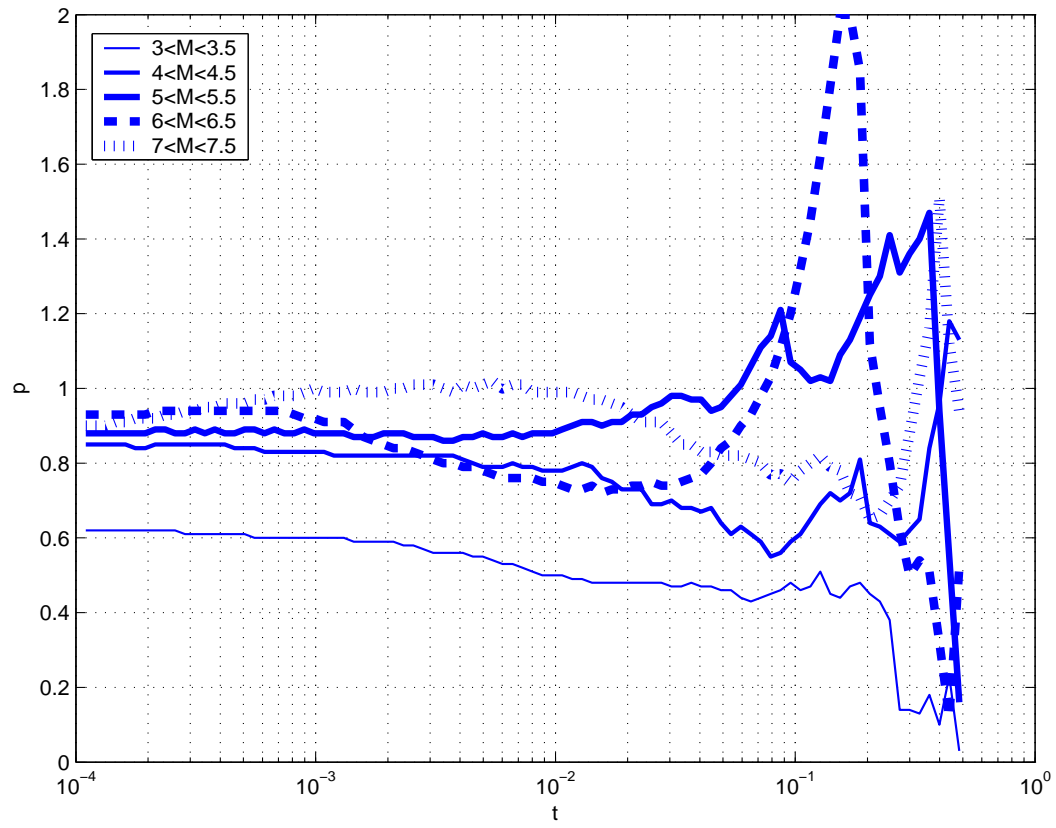


Figure 13. Same as Figure 12 for the post-1932 sub-catalog, using the second declustering technique, with  $R = 2L$ , for different magnitude ranges.

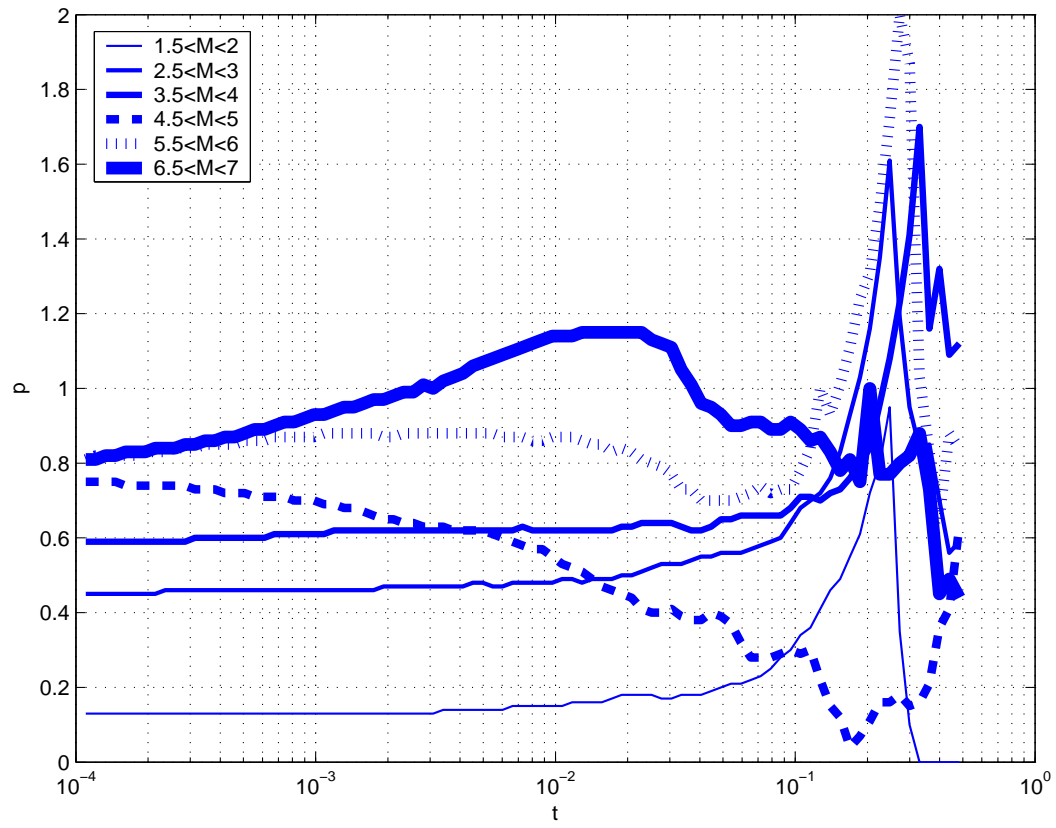


Figure 14. Same as Figure 12 for the post-1994 sub-catalog, using the first declustering technique, with  $R = 2L$ , for different magnitude ranges.

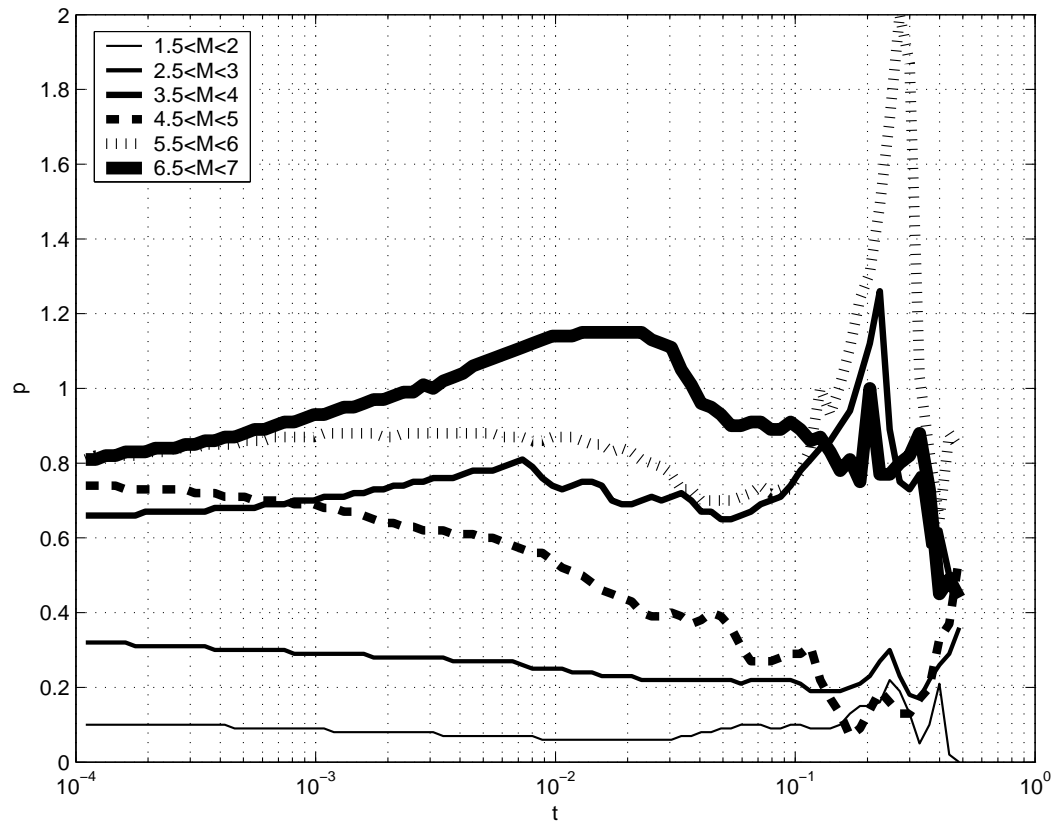


Figure 15. Same as Figure 12 for the post-1994 sub-catalog, using the second declustering technique, with  $R = 2L$ , for different magnitude ranges.

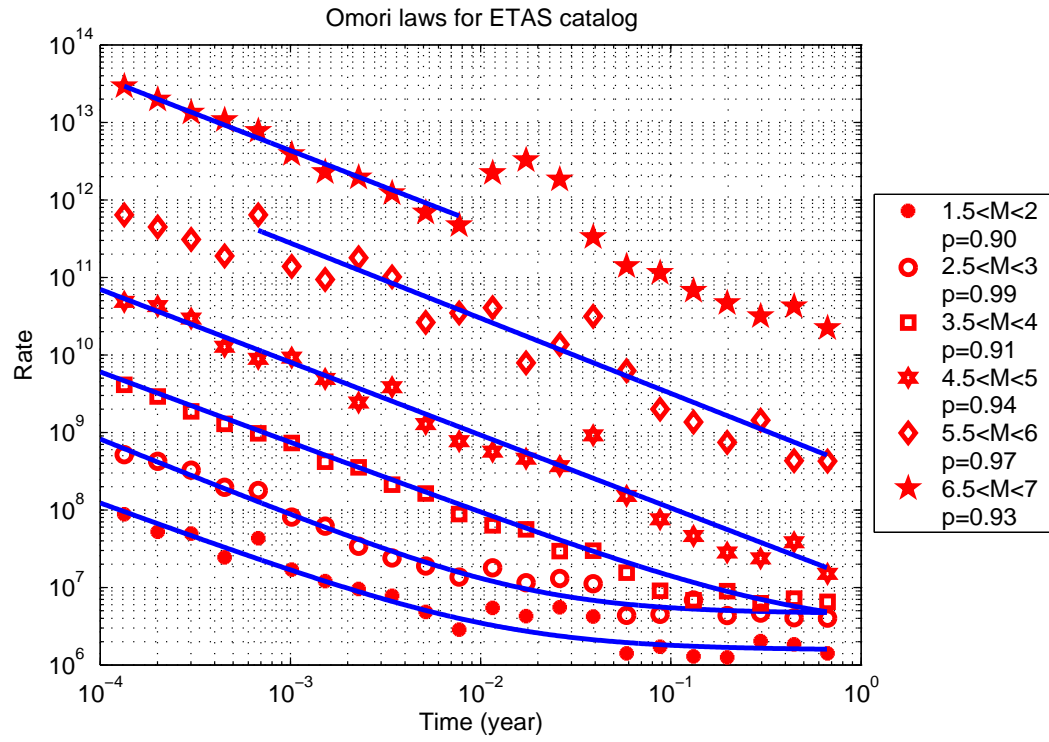


Figure 16. Same as Figure 6 for the synthetic catalog generated with the 3D ETAS model, using the second declustering technique, with  $R = 2L$ , for different magnitude ranges.

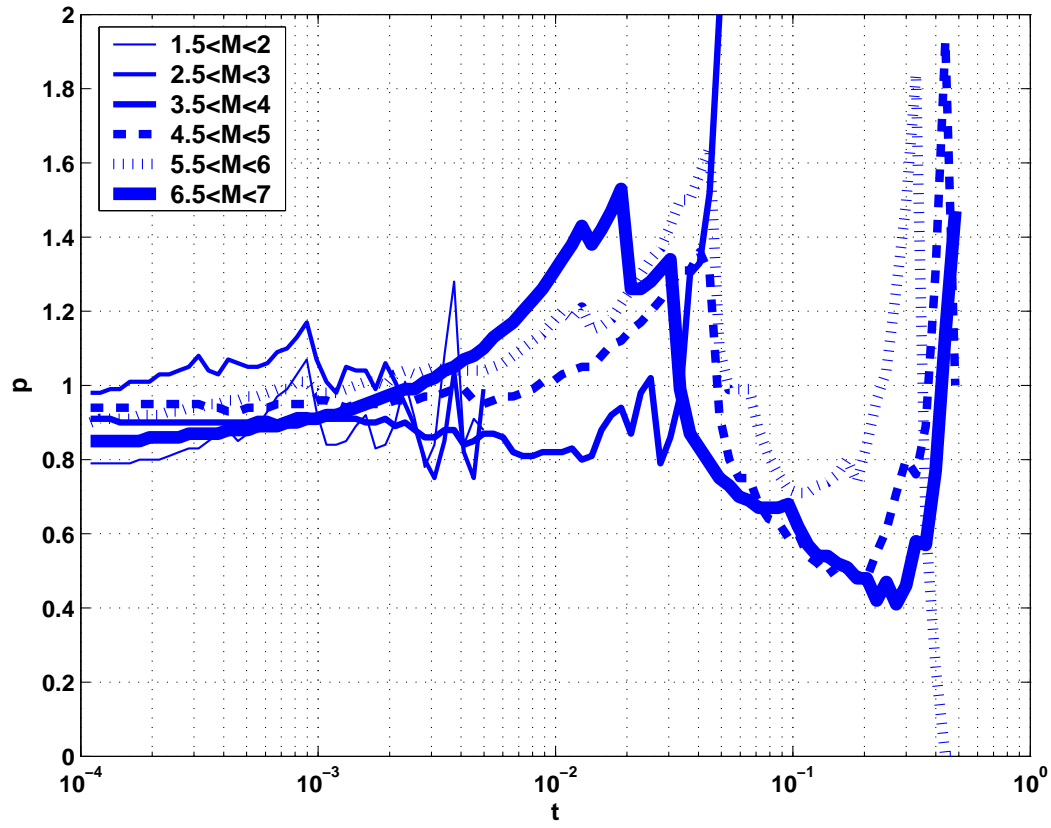


Figure 17. Same as Figure 12 for the synthetic catalog generated with the 3D ETAS model. The MLE formula (44) is applied in a finite time window from  $t$  to  $t_f$ , following the same method as for the real catalogs. The upper value  $t_f$  is 0.01 year for magnitudes up to 3, 0.1 year for the 3.5–4 magnitude range, and 1 year for larger magnitude ranges, so as to minimize bias due to the background seismicity.